Cell Reports

Article

Comprehensive sub-mitochondrial protein map of the parasitic protist *Trypanosoma brucei* defines critical features of organellar biology

Graphical abstract

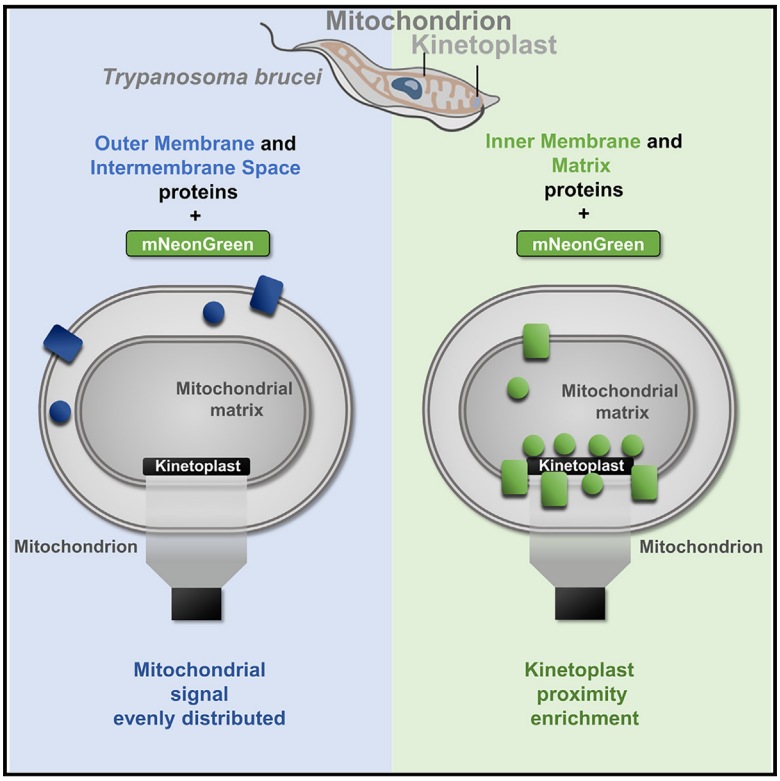

Highlights

- MitoTag localizes 1,053 proteins of *T. brucei* to mitochondrial sub-compartments
- *T. brucei* likely synthesizes fucose in its mitochondrion
- MitoTag predicts protein targeting mode for 781 mitochondrial proteins

Authors

Jan Pyrih, Michael Hammond, Aline Alves, ..., Richard John Wheeler, Keith Gull, Julius Lukeš

Correspondence

jan.pyrih@gmail.com (J.P.), jula@paru.cas.cz (J.L.)

In brief

Pyrih et al. describe a high-confidence mitochondrial proteome (MitoTag) of *Trypanosoma brucei*. The mNeonGreen fluorescent protein tag causes proteins to accumulate near the mitochondrial DNA, allowing the categorization of 1,053 proteins into mitochondrial sub-compartments and mapping of protein targeting mode for the majority of them.

Pyrih et al., 2023, Cell Reports *42*, 113083
September 26, 2023
https://doi.org/10.1016/j.celrep.2023.113083

CellPress

Cell Reports

CellPress
OPEN ACCESS

Article

Comprehensive sub-mitochondrial protein map of the parasitic protist *Trypanosoma brucei* defines critical features of organellar biology

Jan Pyrih,[1,2,3,9,*] Michael Hammond,[1] Aline Alves,[4] Samuel Dean,[5] Jack Daniel Sunter,[4] Richard John Wheeler,[6] Keith Gull,[7] and Julius Lukeš[1,8,*]

[1]Institute of Parasitology, Biology Centre, Czech Academy of Sciences, České Budějovice (Budweis), Czech Republic
[2]Department of Biochemistry, University of Cambridge, Cambridge, UK
[3]Faculty of Science, University of Ostrava, Ostrava, Czech Republic
[4]Oxford Brookes University, Oxford, UK
[5]Division of Biomedical Sciences, Warwick Medical School, University of Warwick, Coventry, UK
[6]Peter Medawar Building for Pathogen Research, Nuffield Department of Medicine, University of Oxford, Oxford, UK
[7]Sir William Dunn School of Pathology, University of Oxford, Oxford, UK
[8]Faculty of Sciences, University of South Bohemia, České Budějovice (Budweis), Czech Republic
[9]Lead contact
*Correspondence: jan.pyrih@gmail.com (J.P.), jula@paru.cas.cz (J.L.)
https://doi.org/10.1016/j.celrep.2023.113083

SUMMARY

We have generated a high-confidence mitochondrial proteome (MitoTag) of the *Trypanosoma brucei* procyclic stage containing 1,239 proteins. For 337 of these, a mitochondrial localization had not been described before. We use the TrypTag dataset as a foundation and take advantage of the properties of the fluorescent protein tag that causes aberrant but fortuitous accumulation of tagged matrix and inner membrane proteins near the kinetoplast (mitochondrial DNA). Combined with transmembrane domain predictions, this characteristic allowed categorization of 1,053 proteins into mitochondrial sub-compartments, the detection of unique matrix-localized fucose and methionine synthesis, and the identification of new kinetoplast proteins, which showed kinetoplast-linked pyrimidine synthesis. Moreover, disruption of targeting signals by tagging allowed mapping of the mode of protein targeting to these sub-compartments, identifying a set of C-tail anchored outer mitochondrial membrane proteins and mitochondrial carriers likely employing multiple target peptides. This dataset represents a comprehensive, updated mapping of the mitochondrion.

INTRODUCTION

The single mitochondrion of trypanosomes has long been at the forefront of revolutionary cell and molecular biology discoveries. Its mitochondrial genome, organized into an extremely complex network of catenated circular molecules termed the kinetoplast,[1] was the first extranuclear DNA ever observed.[2] Transcripts of kinetoplast-encoded protein-coding genes were shown to be post-transcriptionally altered by RNA editing.[3] Initially assumed to be a trypanosome-specific feature, various forms of RNA editing are now known to be widespread in eukaryotes.[4]

Similarly, investigations of respiratory complexes in the mitochondrion of *Trypanosoma brucei* allowed the identification of several novel subunits of the human complex I.[5] Many features of the *T. brucei* mitochondrion facilitate comparative approaches with other systems to address a broad set of questions in evolutionary molecular cell biology. These features include its presence as a single organelle in the cell with dynamic morphology[6] and metabolic changes throughout its life cycle,[7] its protein and tRNA import machineries,[8] ribosome biochemistry,[9] a highly complex respiratory chain,[10] as well as a capacity to modulate its biochemistry on the loss of kinetoplast,[11] and the mechanism of its segregation.[12]

Early studies of the purified mitochondrial proteome (mitoproteome) of *T. brucei*[13,14] were complemented later by an elegant alternative approach, in which the depletion of the outer mitochondrial membrane translocase ATOM40 allowed identification of mitochondrial proteins (mitoproteins) by their decreasing abundance using stable isotope labeling (SILAC) and quantitative proteomics.[15] Unfortunately, all such purification strategies are hindered by varying sets of copurifying or associated non-mitochondrial proteins that cannot be definitively distinguished from genuine organelle components. All proteomics surveys also face intrinsic limitations, such as detection limits of low expressed, short, modified, and/or hydrophobic proteins. Hence, experimental evidence based on the microscopic localization of individual mitoproteins *in cellulo* provides a vital additional route least burdened by false positives.

The mitochondrion has complex sub-compartments due to its double membrane, and proteins may localize to the inner

mitochondrial membrane (IMM), outer mitochondrial membrane (OMM), the intermembrane space (IMS), or the matrix (within the IMM). Mitoproteomes usually lack the detailed resolution of proteins into mitochondrial sub-compartments, as separating IMM, OMM, genomic/transcription locations, and matrix through the cellular fractionation is highly challenging.

Using the mNeonGreen fluorescent protein (mNG),[16] the TrypTag project determined the subcellular localization of the vast majority of proteins encoded in the *T. brucei* genome,[17] being only the fourth such effort in eukaryotes after *Saccharomyces cerevisiae*, *Schizosaccharomyces pombe*, and human cells.[18–20] By analyzing the TrypTag dataset, we have generated a high-confidence mitoproteome of the *T. brucei* procyclic stage, composed of 1,239 proteins. We validated and extended the available mitoproteomes to predict that the complete mitoproteome of *T. brucei* comprises 1,650 proteins.

Furthermore, we characterize an artifact of mNG when in the mitochondrion, which facilitated its use as a tool to distinguish between proteins localized in the matrix and the IMM, as opposed to those in the IMS and the OMM. We categorize 1,053 mitoproteins into these sub-compartments, an unprecedented mapping. Moreover, independent tagging of proteins on both termini allowed us to map the mode of protein targeting into mitochondrial sub-compartments. For example, we identified a specific set of proteins that are either C-tail anchored OMM proteins or are matrix targeted only when their N terminus is fused with mNG. We have also reconstructed poorly defined pathways, such as one-carbon (1C) metabolism operating exclusively in the mitochondrion, and identified new protein components of the tripartite attachment complex (TAC) and the kinetoplast that enabled us to extend the proposed role of TAC to encompass pyrimidine synthesis. Finally, novel functions have been assigned to the mitochondrial sub-compartments, such as the synthesis of fucose and methionine. We believe that our effort represents the deepest analysis of any mitoproteome so far and will be instrumental in further dissections of the evolutionary molecular cell biology of this key organelle.

RESULTS

TrypTag enables the compilation of the most comprehensive *T. brucei* mitoproteome

We identified 1,239 proteins that localized to the mitochondrion when tagged on their N and/or C terminus, which we refer to as MitoTag (Table S1A). On the assumption that there are no false positives, a comparison to other mitoproteomes shows high levels of purity for Panigrahi organelle-purification proteome and Peikert ATOM40 depletome datasets,[13,15] while the Acestor purified mitochondrial proteome[14] possessed a majority of non-mitochondrial proteins and was therefore excluded from further analysis (Figure 1A; Table S1B). The overlap of MitoTag and the mitoproteomes of Panigrahi and Peikert was 546 proteins (Figure 1B; Tables S1B and S1C), with MitoTag identifying 337 novel mitoproteins (Table S1C) while also not containing 411 mitoproteins detected previously.[13,15] Due to the necessity of mitochondrial targeting sequences for a mitochondrial localization, tagging is unlikely to give false positives. The 337 novel mitoproteins were therefore likely refractory to detection by mass spectrometry using the equipment and experimental settings of the aforementioned studies, especially as mass spectrometry sensitivity has increased. As tagged cell lines are generated individually, the latter group (411 mitoproteins) is predominantly a consequence of a failure to generate tagged cell lines or low signal intensity in the tagged cell line (Figure 1B), with a limited number of genuine mitoproteins that were mis-localized. This is consistent with the concept of endogenous *in situ* tagging in TrypTag where gene expression was observed as similar to an endogenous level.[17] We interpret the cell lines with low signal intensity as representatives of weakly expressed mitoproteins. We therefore consider all proteins present in MitoTag, Panigrahi, and Peikert proteomes as true mitoproteins. This yields 1,650 proteins as our best estimate for the total number of proteins in the *T. brucei* procyclic stage mitochondrion.

Enrichment of tagged proteins around the kinetoplast represents an artifact allowing sensitive and specific mapping of mitochondrial sub-compartments

Upon careful examination of MitoTag localizations, we noted that most mitoproteins (903) exhibited an enrichment in the vicinity of the kinetoplast (Figures 2A and S1) that appears similar to previously described kinetoplast antipodal sites.[1,21–23] To investigate this enrichment further, we co-expressed a tagged protein exhibiting this localization (IscU:mNG) with tagged mitochondrial ligase Kβ (Kβ:tdTomato), a marker for the kinetoplast antipodal sites. While the ligase Kβ produced its expected localization,[24,25] IscU only had partial antipodal site overlap, with additional signal along the basal body face of the kinetoplast (Figure 2B), representing a localization not observed previously. We called this distinct localization pattern kinetoplast proximal enrichment (KPE).

As MitoTag exhibited a large cohort of proteins with KPE, we suspected it may represent a tagging-associated artifact, and thus we endeavored to dissect this phenomenon in more detail and ascertain if this cohort contained specific types of proteins. The well-characterized matrix mitoprotein IscU produced KPE when tagged with either mNG (Figure 2C) or an mNG::V5 fusion construct (Iscu:mNG::V5) but not when tagged with only the short, linear V5 epitope tag (IscU::V5), which solely produced a reticulated mitochondrial signal (Figure 2D). A similar result was seen for another five matrix mitoproteins (Figure S2). The KPE was also seen when IscU was tagged with other globular protein tags, such as eGFP, and HaloTag, as well as when mNG was fused directly to the IscU leader sequence (Figures 2C and S3; see Figure S4 for a summary of the different methods used to investigate KPE). The KPE therefore represents an artifact associated with the tagging of a mitoprotein with a globular protein tag.

In addition to the previously mentioned "whole" mitoproteomes that naturally span multiple organelle subdomains, a selection of specific mass spectrometry extractions and analyses have been conducted on specific functional proteins of *T. brucei*, which typically correspond to a single subdomain of the mitochondrion. To understand which mitoproteins exhibited KPE, we mapped its presence or absence onto the mitoribosome (matrix), RNA processing proteins (matrix), respiratory complex machinery (IMM), and the OMM proteome (Figure 3A; Table S1B).[9,10,26–29]

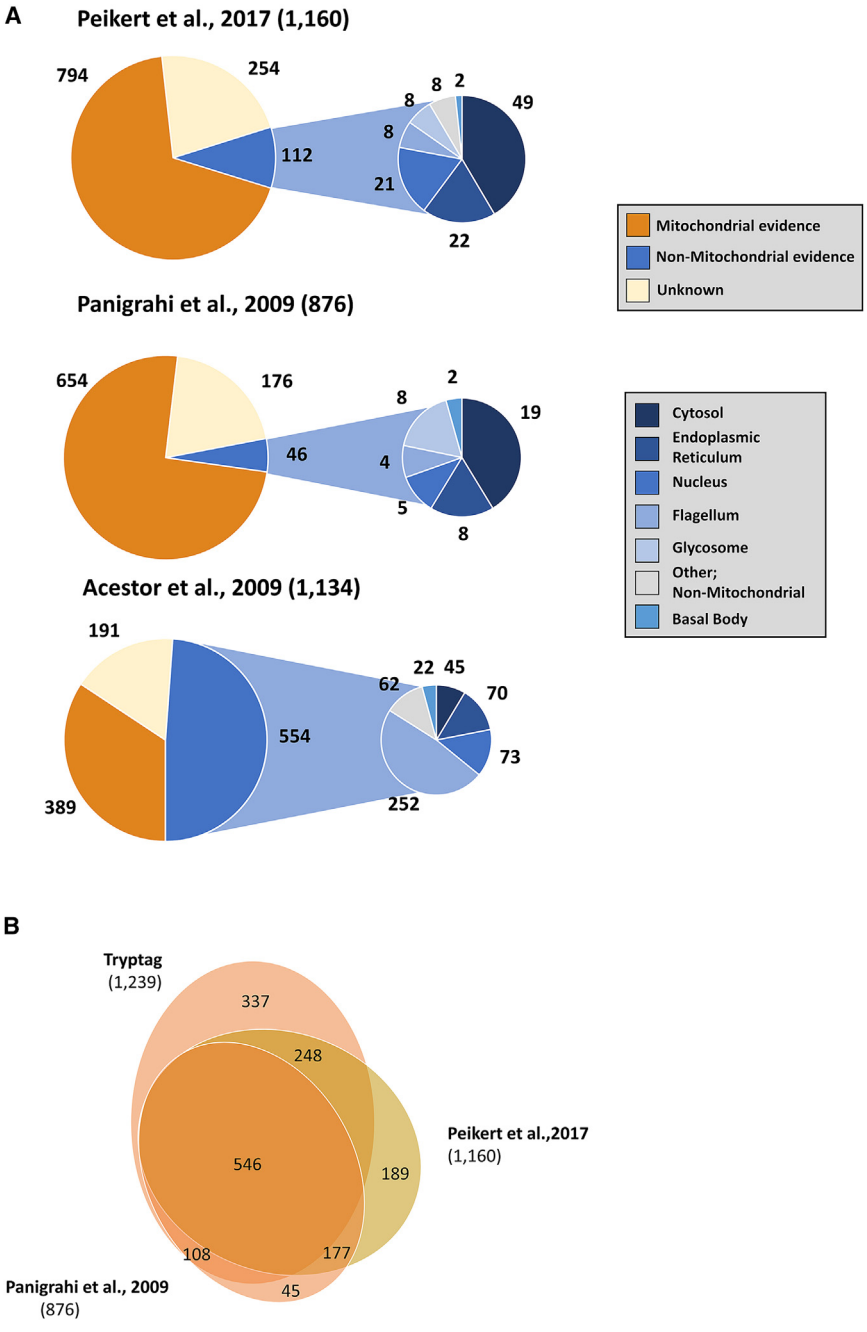

Figure 1. Composition of the *T. brucei* mitoproteome

(A) Previously established mitoproteomes datasets were assessed for purity against TrypTag-defined mitoproteome (MitoTag), with non-mitochondrial proteins further disseminated into top contaminant categories.

(B) Euler diagram of MitoTag against high-purity Peikert and Panigrahi mitoproteomes demonstrating proportions of shared proteins.

Components of both large and small mitoribosomal subunits, RNA processing proteins, and subunits of the respiratory complexes very often had KPE (specificities 100%, 100%, 100%, and 86%, respectively), while the OMM proteins often had noKPE (specificity 82%) (Figure 3A; Table S1B).[9,10,26–29] Combined, this demonstrates that the KPE phenomenon is strongly associated with the matrix and integral IMM proteins (selectivity 96%), while proteins without KPE localize to the OMM and IMS (selectivity 77%) (Figure 3A). Finally, we analyzed the presence or absence of KPE for tagged import and translocation proteins,[30] finding that no OMM proteins (e.g., ATOM40, SAM50) had KPE, while all IMM and matrix proteins except TIM42 and TIM17 proteins displayed KPE (Figures 3B and 3C; Table S1D). Overall, the presence of KPE strongly correlated with a matrix or IMM localization and represents a useful predictive tool.

To experimentally confirm the correlation between the presence of KPE and protein localization in mitochondrial subcompartments, we performed a split-GFP experiment, targeting the first 10 β sheets of GFP (GFP1–10) to the matrix via the IscU target peptide while fusing the final β sheet (GFP11) to mitoproteins with or without KPE (Figure 3D). A fluorescent signal is only expected when GFP1–10 is in the same compartment as GFP11 (the matrix). As a positive control, we measured the fluorescent signal for five selected mitoproteins known to localize to the matrix, IMM, IMS, and OMM. As expected, fluorescence above the background was observed for the matrix and IMM proteins but not for the IMS and OMM proteins (Figure 3E). Screening of 26 additional mitoproteins showed low fluorescence signal (similar to the parental cell line) for proteins whose TrypTag localization lacked KPE. By contrast, fluorescence was significantly higher for the majority of KPE mitoproteins (16/24) (Table S1E; Figure 3E). This further supports the observed correlation between the presence or absence of KPE and the localization of proteins to specific mitochondrial subcompartments.

We then combined the presence/absence of KPE in combination with the TM domain prediction to determine the mitochondrial sub-compartment of each tagged mitoprotein from TrypTag, termed the "KPE/TM mitochondrial sub-compartment classification strategy" (Figure 3F; Table S1F). Proteins with KPE and predicted TM domains were classified as integral IMM proteins (159 proteins), while those without a TM domain were classified as matrix proteins (either as soluble components or as

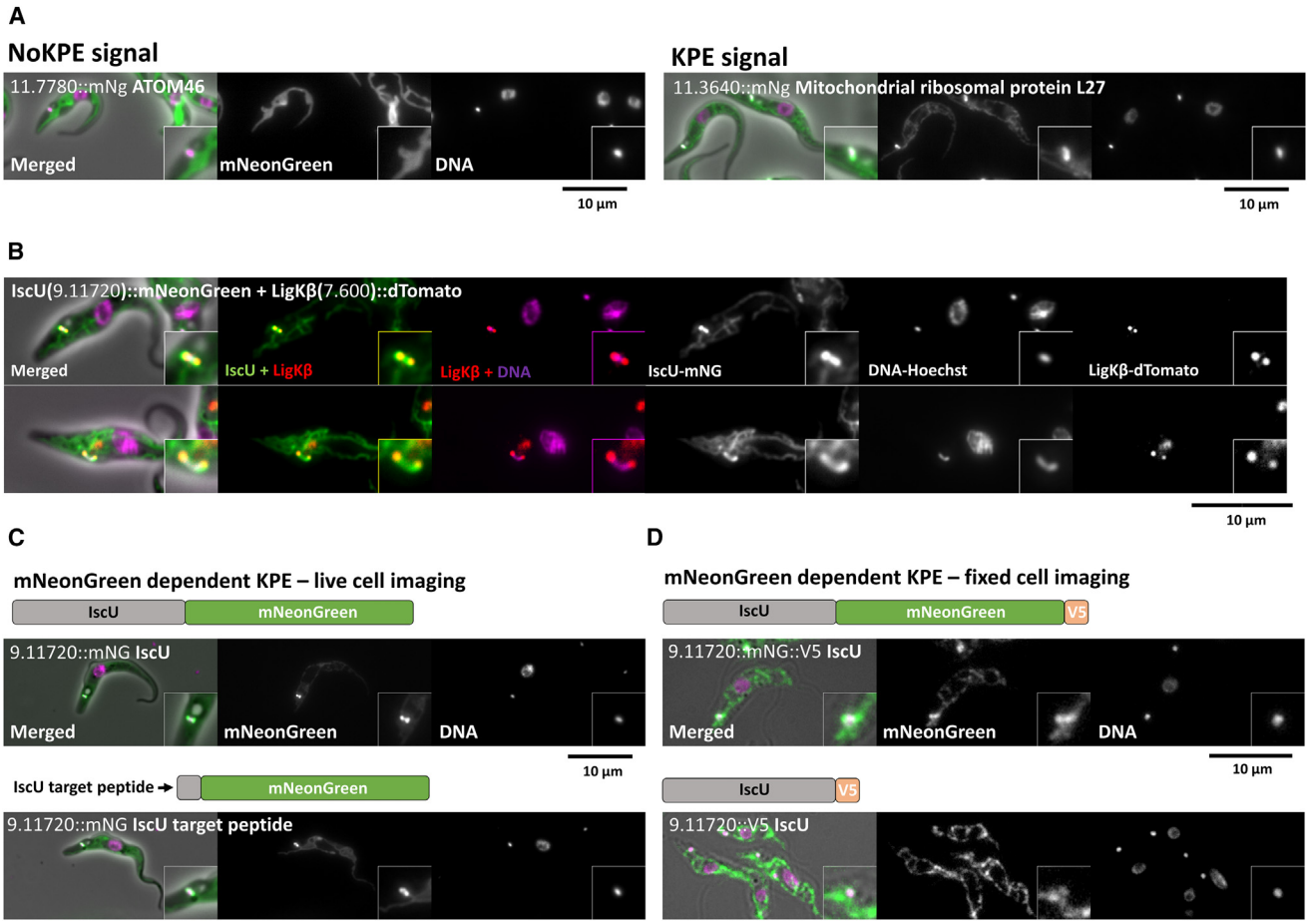

Figure 2. Characterization of kinetoplast proximal enrichment recorded from MitoTag

The scale bar represents 10 µm, with a 2-fold magnification of the kinetoplast insets.

(A) Comparison of cell lines with and without kinetoplast proximal enrichment (KPE). Unless indicated otherwise, from left to right, microscope image panels show phase contrast merged with fluorescence overlay, mNeonGreen (mNG) fluorescence, and Hoechst-stained DNA. Insets zoom in on the kinetoplast region.

(B) Dual tagging of IscU with mNG and ligase Kβ (Tb.927.7.600) with dTomato, demonstrating KPE (tagged with mNG) association with the antipodal sites (tagged with dTomato).

(C) Live cell imaging of tagging approaches against full-size IscU (Tb927.9.11720) with mNG, and mNG fused only to the target peptide of IscU.

(D) Immunofluorescence of fixed cells expressing IscU tagged with either mNG and/or V5 tag.

peripheral IMM proteins facing the matrix) (757 proteins) (Figure 3F). NoKPE proteins that possess a predicted TM domain were classified as integral OMM components (89 proteins), while those lacking a TM domain localize to either the IMS (as soluble proteins or as components of either membrane facing the IMS) or as the cytosol-facing proteins attached to the OMM (48 proteins) (Figure 3F). This high-coverage mapping represents the first time it has been possible to comprehensively map the sub-compartmental composition of the majority of proteins in this organelle.

Matrix-localized 1C metabolism, methionine, and fucose synthesis

While the *T. brucei* mitochondrion represents a highly studied organelle, we wondered whether the newly discovered mitoproteins together with our KPE/TM mitochondrial sub-compartment classification strategy would provide new insights into metabolic pathways (Figure 4A). One such pathway, 1C metabolism, typically converts and exchanges folate intermediates between the mitochondria and the cytosol, playing an essential role in DNA biosynthesis, mitochondrial protein translation, and amino acid homeostasis and redox defense.[31,32,33] Contrasting with other eukaryotes, including the closely related *Leishmania* spp.,[31,34] our reconstruction of 1C metabolism showed it is confined to the mitochondrial matrix, lacking equivalent metabolic steps in the cytosol (Figure 4; Table S1G).

We identified additional pathways linked to 1C metabolism. For the first time, we localized 5-methyltetrahydropteroyltriglutamate-homocysteine S-methyltransferase (Tb927.8.2610) within the matrix (Figure 4). This raises the possibility that this enzyme is involved in methionine synthesis coupled with direct recycling of homocysteine. This is further supported by our localization of thiopurine S-methyltransferase (Tb927.5.3000) in the matrix, as well as the presence of homocysteine-recycling cystathionine β-synthase (Tb11.02.5400) in the ATOM40 importome.[15] The

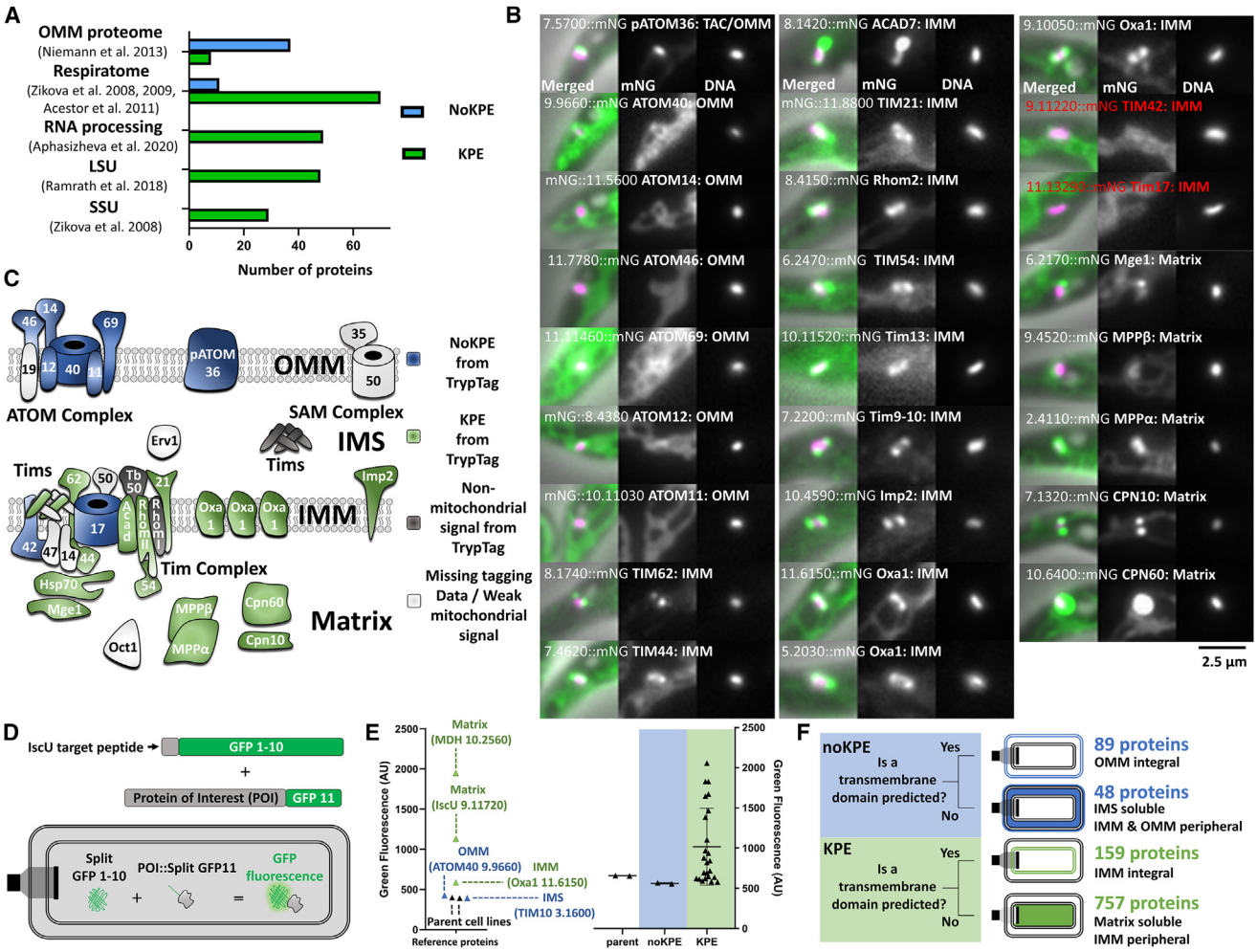

Figure 3. Use of KPE and NoKPE categories to sort mitoproteins into sub-compartments

The scale bar represents 2.5 μm.

(A) Number of proteins from each sub-mitochondrial proteome that display KPE or noKPE signal in MitoTag. Proteins with no data, no expression signal, or with only background mitochondrial signal are not displayed.

(B) Kinetoplast-focused cell lines showing mitochondrial import machinery that displays either KPE or NoKPE; established localization is displayed next to protein name. Red font indicates mitoproteins with TrypTag localization conflicting with previous studies (Tim42 and Tim17 lack KPE seen in other integral IMM proteins). Unless indicated otherwise, from left to right, microscope image panels show phase contrast merged with fluorescence overlay, mNG fluorescence, and Hoechst-stained DNA. Full information and GI numbers of proteins are in Table S1D.

(C) Model of mitochondrial protein import machinery in *T. brucei*, colored to indicate KPE correlation with matrix and integral inner membrane proteins. Dark gray coloring indicates proteins assigned as non-mitochondrial (Tim50 is localized to the basal bodies, while three other proteins—rhomboid protein I, Tim10, and Tim8-13—localize in the cytosol).

(D) Scheme of split-GFP verification experiment. GFP1–10, first 10 β-sheets of GFP; GFP11, 11th β sheet of GFP. The intensity of measured GFP fluorescence correlates with KPE.

(E) Split-GFP experiment tested against marker proteins with known mitochondrial sub-compartment and parental cell lines. Green and blue texts indicate proteins exhibiting KPE and noKPE, respectively (left panel). Fluorescence values of proteins with unknown localization exhibiting noKPE or KPE (right panel). List of proteins surveyed in Table S1D. Mean values and standard deviation are visualized in the graph.

(F) Sorting strategy for predicting the sub-compartments for proteins exhibiting either KPE or noKPE in MitoTag along with the number of proteins belonging to each category.

generated methionine is likely needed for folate-dependent N-formylmethionine tRNA synthesis in the 1C metabolism cycle, which would represent a mitochondrial adaptation not reported previously. It was hypothesized recently that in *T. brucei,* 1C metabolism-dependent dUTP synthesis was orchestrated via an interplay of enzymes distributed in the mitochondrion, cytosol, and nucleus.[35] In contrast to what was predicted, the mitochondrion appears capable of dUTP and dUDP synthesis through deoxyuridine 5′-triphosphate nucleotidohydrolase (dUTPase) present in both mitochondrial matrix and nucleus (Figure 4).

In mammals, fucose is synthesized in the cytoplasm,[38] while in *T. brucei*, homologs of three key synthesis enzymes

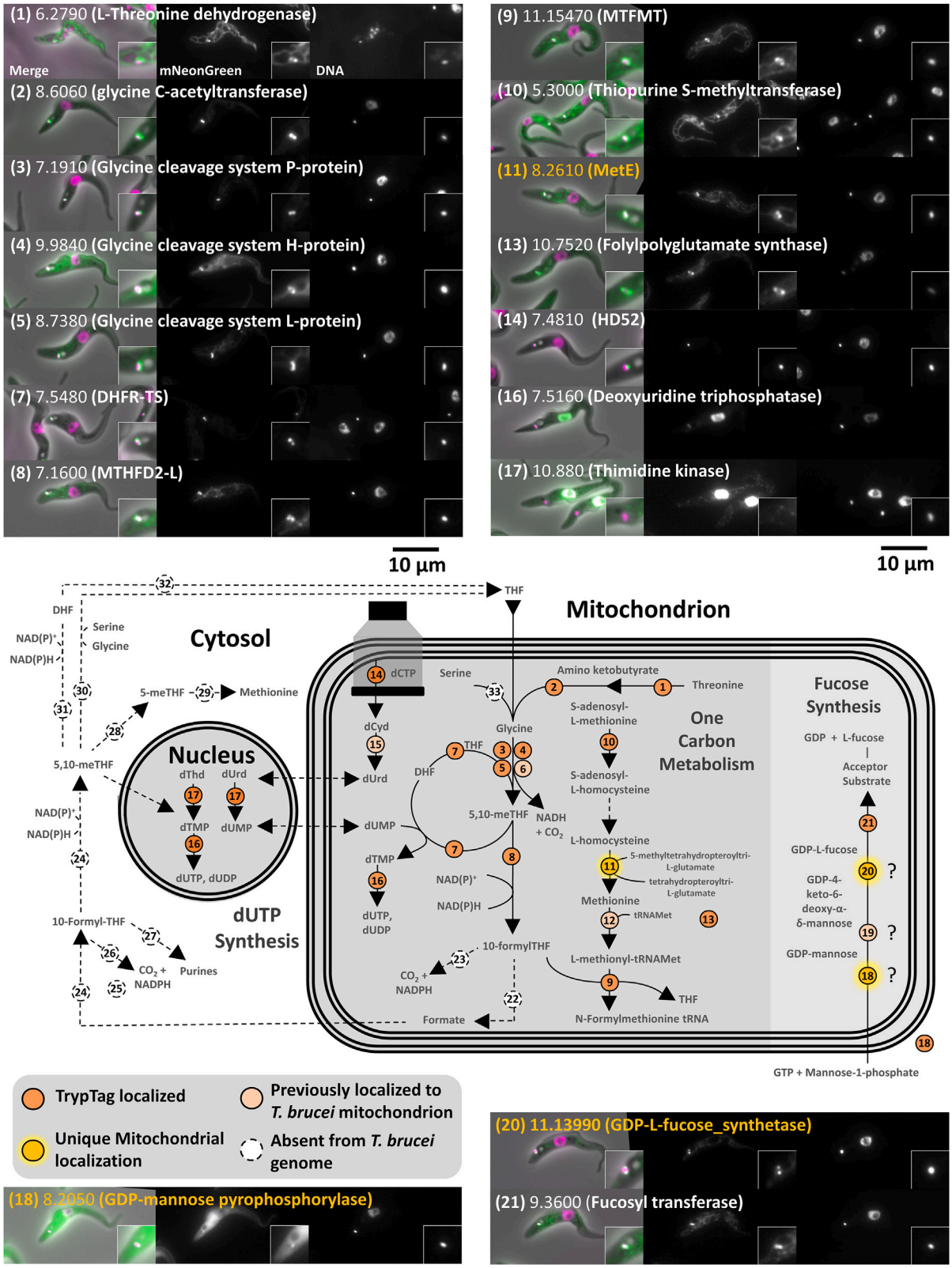

(legend on next page)

(GDP-mannose pyrophosphorylase, GDP-L-fucose synthetase, and GDP-mannose 4,6 dehydratase) localize to the glycosomes,[36,37] and the fucose synthesis pathway is largely expected to be glycosomal.[37] However, we observed evidence for mitochondrial localization of at least parts of the late fucose synthesis pathway. GDP-L-fucose synthetase (Tb927.11.13990) localized to the matrix (Figure 4) in a characteristic manner. GDP-mannose pyrophosphorylase (Tb927.8.2050) was present in the cytoplasm and mitochondrial matrix (see mitoproteins with dual localizations below; Figure 4; Table S1G). Along with other data interpretations, this suggests that the fucose used by the recently identified mitochondrial fucosyltransferase (FUT1)[39,40] is possibly also synthesized within the mitochondrion.

Identification of six novel kinetoplast-associated proteins

The kinetoplast is a fascinating mitochondrial structure typical of kinetoplastid protists. To our knowledge, 57 proteins have been identified localizing to complex kinetoplast-associated structures by a range of approaches (Table S1D).[1,12,41] The similarity of KPE to the antipodal sites and kinetoflagellar centers prevented unambiguous assignment of proteins to these structures. Therefore, we considered all "two-dotted" signals in the proximity of the kinetoplast as KPE, which correlated well with the presence of 10 previously characterized components of the antipodal sites in this category (Table S1D). To extend our knowledge of the kinetoplast biology, we thoroughly analyzed the MitoTag for the presence of fluorescent signal near the kinetoplast that does not exhibit a two-dotted pattern, which could reflect the association of tagged proteins with the TAC and kinetoplast disk (Figure 5A; Table S1D). We identified 24 such proteins, out of which 18 were previously localized to the TAC or kinetoplast disk, with six reported for the first time (Figure 5B). While the majority of the newly identified kinetoplast/TAC candidates have no predicted function, one protein, HD52 (Tb927.7.4810), was recently linked with both kinetoplast segregation and dUMP synthesis.[42] Our identification of this protein in the kinetoplast/TAC region validates our experimental approach and additionally links the kinetoplast region directly with dUMP synthesis and 1C metabolism for the first time (Figure 4).

The distance between the Hoechst-stained kinetoplast and fluorescent signal of a tagged protein has been used previously to define the intramitochondrial distribution of TAC proteins.[43,44] We used a semiautomatic algorithm to determine the distance between the fluorescent protein signal and the kinetoplast. Based on the measured distance, proteins were classified as (1) flagellar proximal TAC, (2) middle TAC, and (3) kinetoplast proximal TAC and/or kinetoplast (Figure 5C). The predicted positions of known TAC and kinetoplast components were consistent with previous literature[43] (Figure 5C). We observed that the majority of newly identified components are proximal to the kinetoplast.

Insights into modes of mitochondrial import

Although the majority of mitoproteins employ N-terminal target peptides, there is an expanding subset of proteins known to use C-terminal signals, which primarily direct proteins into the OMM.[45] Trypanosome protein targeting machinery comprises both highly divergent homologs of eukaryotic proteins and proteins that appear unique to kinetoplastid protists. Some of those proteins were proposed to functionally replace original eukaryotic proteins that are absent.[46] Therefore, we decided to study this mitochondrial import in greater detail. The tagging of many *T. brucei* mitoproteins at both termini allowed us to investigate at which terminus the target peptide likely resides, based on the assumption that the mNG tag would disrupt the targeting signal present at the tagged terminus. Equally, successful mitochondrial targeting on both termini would suggest the presence of an internal target peptide.

To avoid ambiguous cases where proteins localize to the mitochondrion when tagged at one terminus and a different organelle when tagged at the other, i.e., cases where multiple competing targeting sequences to different organelles may be present, we only analyzed proteins where both N- and C-terminal tagging gave either mitochondrial, cytoplasmic, or no signal. We identified 781 proteins satisfying these criteria (Table S1H), and our data predict that, of these, 632 have an N-terminal targeting sequence (81%), 37 have a C-terminal one (4.7%), and 112 employ targeting sequences that appear to be functional in a non-terminal position (14.3%).

We then further categorized each terminus individually using our KPE/TM mitochondrial sub-compartment classification strategy (Figures 6A and 6B). A large majority of matrix mitoproteins (445; 89.3%) are predicted to possess N-terminal targeting signal, with only six proteins entering the matrix via a C-terminal target peptide (Figures 6A and 6B). A further 47 matrix proteins localized to the matrix when tagged on either terminus. These

Figure 4. One-carbon metabolism and fucose synthesis metabolic pathways

The scale bar represents 10 μm, with a 2-fold magnification of the kinetoplast insets. Gold labeling indicates proteins localized in the mitochondrion for the first time, which are additionally not documented in mitochondria of other organisms. Scheme for one-carbon (1C) metabolism is based on Ducker and Rabinowitz.[31] Four proteins (indicated in peach) localized to the mitochondrion based on previously published data, but they are not visualized in TrypTag: (6) GCS-t, glycine cleavage system protein T (Tb927.11.9670);[13,15] (15) CDA, cytidine deaminase (Tb927.9.3000);[35] and (19) GMD, GDP-mannose 4,6 dehydratase (Tb927.10.15490).[15] For (12) MetRS, methionyl-tRNA synthetase (Tb927.10.1500: MetRS), TrypTag data visualized a cytosolic location, but it was previously shown to be dually localized in the mitochondrion and the cytosol.[15] Additionally, the question mark next to the fucose synthesis proteins represents the former identified location in glycosomes.[36,37] MetE, 5-methyltetrahydropteroyltriglutamate-homocysteine S-methyltransferase; (22) MTHFD1L, NADP+-dependent methylenetetrahydrofolate dehydrogenase 1-like protein; (23) ALDH1L2, mitochondrial 10-formyltetrahydrofolate dehydrogenase; (24) MTHFD1, methylenetetrahydrofolate dehydrogenase 1; (25) FPGS, folylpolyglutamate synthase; (26) ALDH1L1, aldehyde dehydrogenase 1 family member L1; (27) GART, phosphoribosylglycinamide formyltransferase/ATIC, 5-aminoimidazole-4-carboxamide ribonucleotide formyltransferase/IMP cyclohydrolase; (28) MTHFR, methylenetetrahydrofolate reductase; (29) MTR, methionine synthase; (30) SHMT1, cytosolic serine hydroxymethyltransferase; (31) TS, thymidylate synthase; (32) DHFR, dihydrofolate reductase; (33) SHMT2, mitochondrial serine hydroxymethyltransferase. From left to right, microscope image panels show phase contrast merged with fluorescence overlay, mNeonGreen fluorescence, and Hoechst-stained DNA.

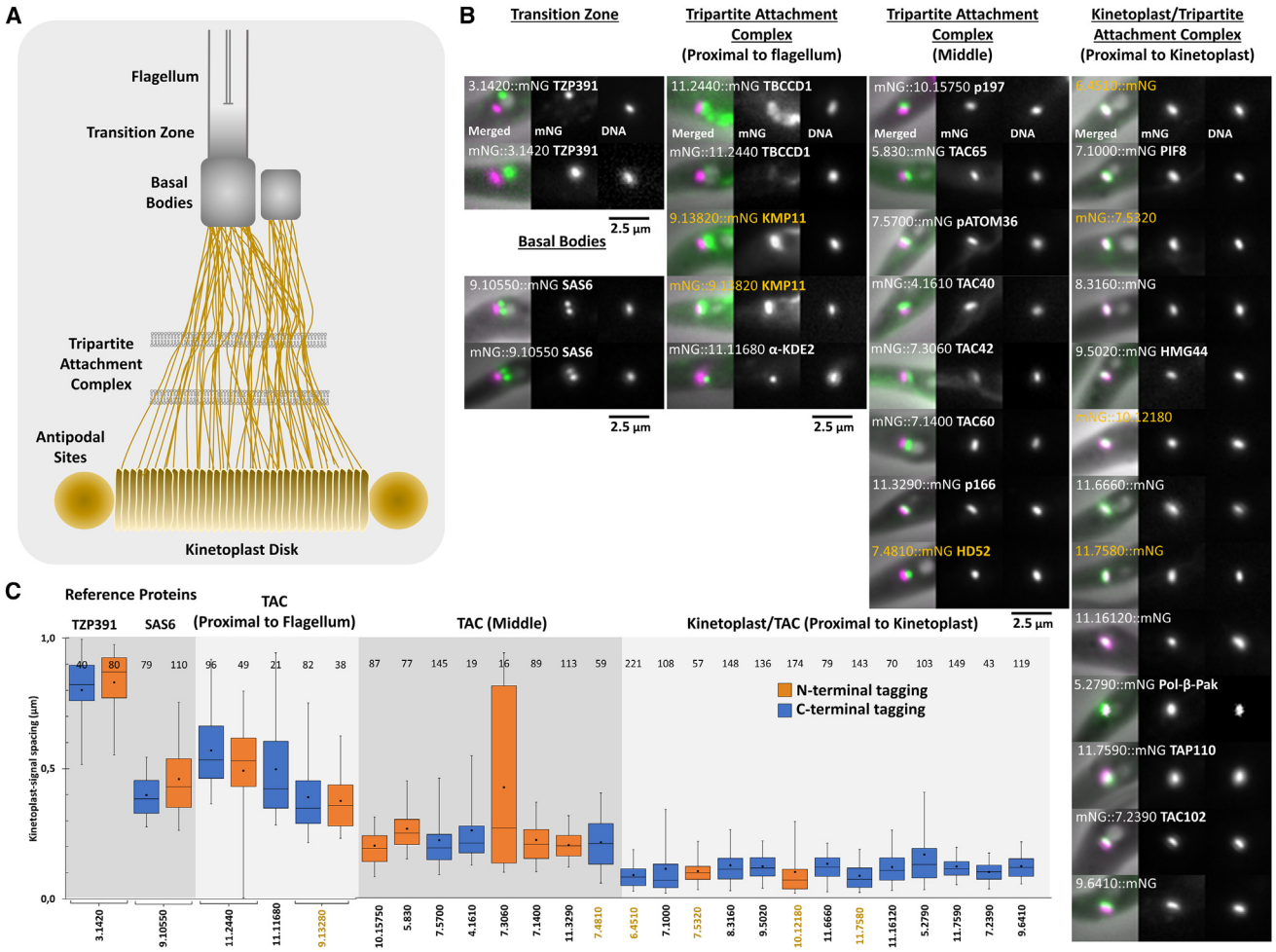

Figure 5. Sorting of proteins localizing in the kinetoplast/TAC area

The scale bar represents 2.5 µm.

(A) Schematized depiction of distinguished sub-compartments within the kinetoplast/TAC area.

(B) Assignment of proteins into the sub-compartments. Gold font indicates novel proteins localized for the first time based on TrypTag. From left to right, microscope image panels show phase contrast merged with fluorescence overlay, mNG fluorescence, and Hoechst-stained DNA. Insets zoom in on the kinetoplast area.

(C) Graph depicts the measured distance between the kinetoplast and the fluorescence signal of individual sub-compartmentalized proteins. Mean values and standard deviation are visualized. The number of cells measured is indicated for each measurement.

observations demonstrate the predominance of N-terminal target peptides for matrix localization. Of the six C-terminal target peptide dependent matrix proteins, three are associated with the kinetoplast, including the antipodal site component topoisomerase II (Tb927.9.5590), RNA-editing 3′ terminal uridylyl transferase 1 (Tb927.7.3950), and a hypothetical protein (Tb927.7.5320) localized to the kinetoplast in this study (Figure 5), implying a putative C-terminal-dependent targeting mechanism for a subset of kinetoplast-associated proteins (Figure 6C).

Interestingly, based on presence/absence of KPE, seven proteins localize to different mitochondrial sub-compartments depending on the tagged terminus (OMM upon N- and IMM upon C-terminal tagging) (Figure 6D; Table S1H). We suggest this is due to the presence of two target peptides, one internal, targeting the OMM, and another N-terminal, subsequently targeting the IMM. Upon N-terminal tagging, the protein is immobilized in the OMM (Figure 6D). Such behavior was previously described for certain mitochondrial carrier proteins in yeast,[47,48] and indeed, three out of these seven proteins are mitochondrial carriers (Table S1H). We identified a further seven candidate proteins where N- and C-terminal tagging results gave noKPE and KPE signals, respectively, therefore suggesting a similar targeting mechanism. Although these proteins were not predicted to possess a TM domain, this most likely represents false negatives of the TM prediction algorithms, as two are annotated as mitochondrial carriers, and one is an integral subunit of complex I (Table S1H).

We identified six OMM proteins whose mitochondrial localization was disrupted by only C- terminal tagging. As expected, these proteins had a single C-terminal TM domain that could

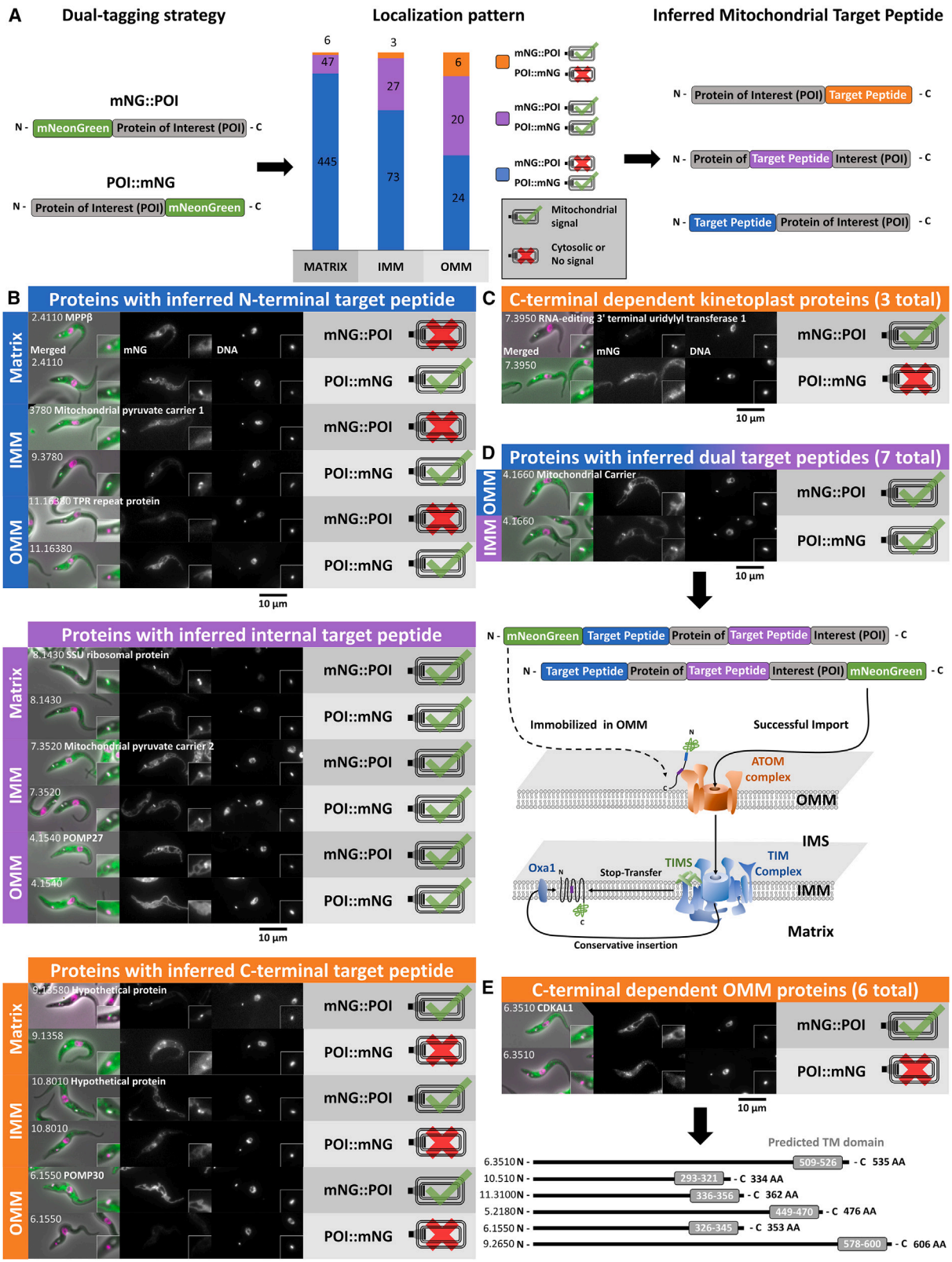

(legend on next page)

potentially act as an OMM anchor (Figure 6E). One is a homolog of threonylcarbamoyladenosine tRNA methylthiotransferase (CDKAL1; Tb927.6.3510), and it was also detected in the importome and OMM proteomes.[15,27] In most eukaryotes, CDKAL1 is anchored to the endoplasmic reticulum membrane[49–51] and hence represents a notable retargeting event. Ultimately, tracking the modes of mitochondrial import through combining KPE/TM mitochondrial sub-compartment classification strategy with tagging terminus information produced specific subsets of mitoproteins that are informative to understanding the evolution of mitochondrial import machinery.

Mitoproteins with dual localization

A small subset of mitoproteins simultaneously localized to an additional cellular compartment: two to the nucleus and nine (including GDP-mannose pyrophosphorylase) to the cytoplasm, all in addition to the mitochondrial matrix. Seven of these have not been previously reported to have such localization (Figure 7; Table S1A). Trypanosomes employ trypanothione and trypanothione reductase for the breakdown of hydrogen peroxide through the action of tryparedoxin-dependent peroxidases.[52] We found trypanothione reductase (Tb927.10.10390) and one trypanoredoxin peroxidase (Tb927.7.1140) in both the mitochondrial matrix and the cytoplasm (Figure 7C; Tables S1 and S7), opening the possibility that they act upon not only cytosolic but also mitochondrial trypanoredoxins, contrary to claims by Ebersoll et al.[53] Two core tricarboxylic acid (TCA) enzymes (aconitase, isocitrate dehydrogenase) and two additional proteins linked to this cycle (alanine aminotransferase and aspartate aminotransferase) localized to both the cytosol and the mitochondrial matrix (Figure 7C). Apart from aconitase,[54] dual localization of the TCA cycle enzymes has not been reported for *T. brucei*.[55–57] These dually localized TCA and redox enzymes shed light on where these pathways may additionally operate.

DISCUSSION

T. brucei arguably possesses the most well-investigated protist mitochondrion, yet despite multiple previous proteomics surveys, our genome-wide protein tagging analysis identified 337 novel mitoproteins, in addition to a strong agreement with previous proteomic analyses. We were able to assemble the most comprehensive *T. brucei* mitoproteome to date. Given the requirements of mitoproteins for proper import primarily via target peptides, tagging of non-mitochondrial proteins is unlikely to produce entry to the organelle—a false positive. However, the disruption of targeting signals via adjacent epitope tags more likely poses the risk of preventing proper mitochondrial import (false negatives). Awareness of such issues is fundamental to appreciating such global genomic surveys. We note that mitochondrial localization of several well-characterized mitoproteins, including cytochrome *c* oxidase assembly factor 6 and mitochondrial Hsp70, was not observed. This was generally either due to the failure to generate a cell line, no signal being detected in the cells, or (in the case of these two examples) a non-mitochondrial location being recorded for the N-terminal tagged version. Varied complementary methodologies are therefore important for interrogating the mitoproteome of any eukaryote. The total mitoproteomic complexity estimated from this study is comparable to the largest known mitoproteomes of the closely related flagellate *Euglena gracilis* (1,756)[58] and the distantly related *Homo sapiens* (1,626).[59]

Tagging aberrations can, however, be informative in an organelle context: differences between N- and C-terminal tagging allowed mapping of the position of targeting sequences, and the KPE artifact stemming from a globular tag allowed global and highly accurate mapping of mitochondrial sub-compartments. We mapped target peptides across the mitoproteome, identifying canonical N-terminal targeting, C-terminal OMM anchoring, and putative internal targeting sequences. Moreover, we mapped cases where tagging led to a probable arrest of several typical IMM proteins in the OMM upon N-terminal tagging (Figure 6D). In yeast, internal non-cleavable sequences of mitochondrial carriers are recognized by Tom70 of the TOM complex,[47,48] allowing them to pass through the OMM by employing their N-terminal signals.[45] In *T. brucei*, Tom70 is absent, but the lineage-specific non-homologous ATOM69, copurifying with the TOM complex, was proposed to mimic its function.[8] Arrested import may reflect proteins binding to ATOM69, followed by arrested relocation to the IMS, and subsequently IMM, due to the presence of an N-terminal mNG.

The molecular mechanism that causes KPE remains elusive and requires further study to be completely elucidated. Nevertheless, we were able to demonstrate that accumulation of hundreds of mitoproteins near the kinetoplast is most likely not their genuine localization, which raises concerns about previously identified proteins in kinetoplast-associated structures, particularly in the antipodal sites, based on fluorescent protein tagging,[21–23,60,61] warranting their revalidation by different tags or monoclonal antibodies in the future. A similar ambiguity potentially applies for antipodal and kinetoflagellar center proteins in *Crithidia fasciculata*[62] and *Leishmania tarentolae*.[63]

Figure 6. Scheme of N- and C-terminal tagging strategies resulting in inferences on mitoprotein localization

The scale bar represents 10 μm, with a 2-fold magnification of the kinetoplast insets.

(A) Proposed mode of protein targeting based on mNeonGreen interference with mitochondrial protein targeting machinery. Matrix, IMM, and OMM categories were assigned based on KPE and noKPE categories, as well as predicted transmembrane domains (see Figure 3F).

(B) Examples of localization patterns present in each mitochondrial sub-compartment.

(C) Representative matrix protein sub-localized to the kinetoplast with C-terminal-dependent targeting isdisplayed.

(D) Representative cell line for N-terminally tagged IMM proteins displayed only partial mitochondrial delivery, as they likely become immobilized in the OMM. Schematics shows mode of proposed OMM immobilization of aforementioned N-terminally tagged proteins versus delivery to the IMM upon C-terminal tagging. We propose that the internal targeting peptide first docks the entire protein on the OMM receptor protein, and then the N-terminal targeting peptide facilitates the insertion into the membrane.

(E) Representative cell line for C-terminal import-dependent protein that localizes to the OMM. From left to right, microscope image panels show phase contrast merged with fluorescence overlay, mNG fluorescence, and Hoechst-stained DNA.

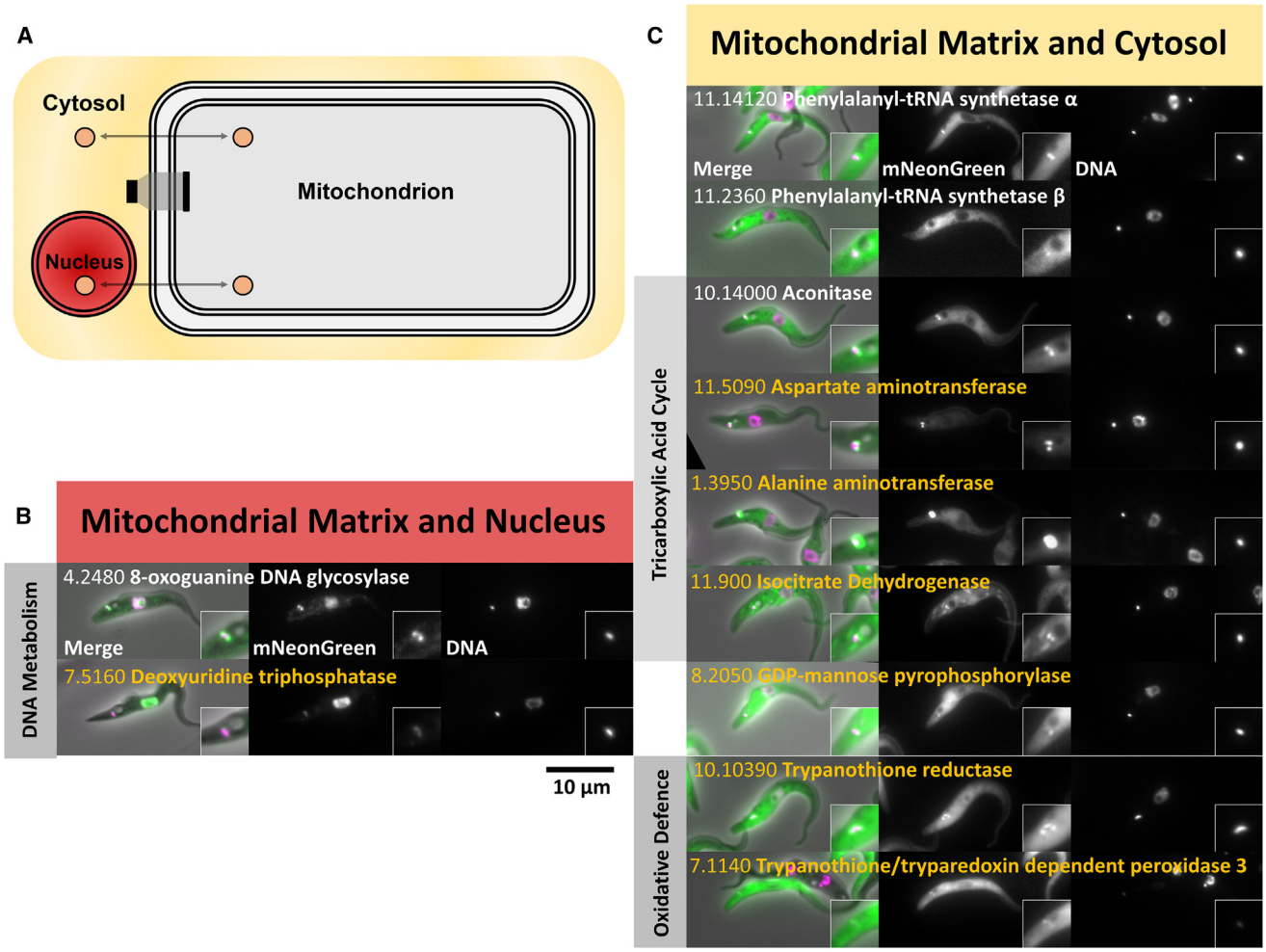

Figure 7. Proteins with dual localization

The scale bar represents 10 μm, with a 2-fold magnification of the kinetoplast insets.

(A) Depiction of selected proteins displaying dual localization—in the mitochondrion and in another cellular compartment.

(B) Proteins shared between the mitochondrion and the nucleus.

(C) Proteins shared between the mitochondrial matrix and the cytosol. Gold text indicates proteins with novel dual localization established by TrypTag. From left to right, microscope image panels show phase contrast merged with fluorescence overlay, mNG fluorescence, and Hoechst-stained DNA.

Interestingly, the vast majority of IMM proteins, irrespective of expected orientation in the membrane, displayed KPE. This suggests that even IMM proteins in transit with the tag transiently exposed to the matrix become enriched near the kinetoplast, which in turn, informs the likely mechanism of targeting. Yeast mitochondria use two pathways to incorporate integral proteins into their IMM: either the stop-transfer mechanism, inserting proteins directly from the IMS, or the conservative mechanism, which passes proteins through the IMM into the matrix and mediates insertion via Oxa1 (Figure 6D).[45] The observation of near-universal KPE for IMM proteins in *T. brucei* (Table S1D) suggests that the conservative mechanism predominates, perhaps associated with adaptations of its inner membrane translocation machinery, such as the lack of a typical TIM22 complex,[8] and the presence of three rather than one ortholog of Oxa1 (Table S1D).

The identification of six new kinetoplast-associated proteins is significant for such an intensely studied structure of the trypanosome mitochondrion. One such protein, HD52, links *de novo* synthesis of pyrimidines with the kinetoplast, which may contribute toward its more efficient replication and transcription. We also identified a possible metabolic connection between the mitochondrion and the cytoplasm via the TCA cycle and its associated enzymes aspartate and alanine aminotransferases. Previously considered non-functional, instead we can suggest that aspartate and alanine aminotransferases short circuit the TCA cycle by using pyruvate and glutamate as substrates to synthesize α-ketoglutarate directly from oxalacetate, reminiscent of some bacteria and mammalian cancer cells.[64,65]

Our data show that 1C metabolism operates exclusively in the mitochondrial matrix, raising the possibility of its linkage with mitochondrial methionine synthesis/recycling from homocysteine via

5-methyltetrahydropteroyltriglutamate-homocysteine S-methyltransferase. This represents a candidate for lateral gene transfer from bacteria not previously identified as mitochondrial.[66,67] Moreover, we propose that the conversion of tetrahydrofolate to 5,10-methylenetetrahydrofolate occurs without serine hydroxymethyltransferase, being mediated only by the glycine cleavage system (Figure 4). The glycine needed for this step is likely being synthesized from threonine through L-threonine dehydrogenase and glycine C-acetyltransferase, similar to human stem cells.[31]

Interestingly, the localization of fucose synthesis pathway extends beyond the glycosomes and likely includes the mitochondrion, which is a notable observation as this compartment's involvement has not been previously identified in any other species. A mitochondrial fucosyltransferase (FUT1) was recently identified using antibodies against recombinant protein,[39] and it now seems likely that its fucose substrate is synthesized *in situ*. The final steps of fucose biosynthesis involve three enzymes (Figure 4): GDP-mannose pyrophosphorylase, GDP-mannose 4,6-dehydratase, and GDP-L-fucose synthetase. The tagging of GDP-mannose pyrophosphorylase and GDP-L-fucose synthetase produced a pattern highly indicative of a mitochondrial localization, and presence of the latter protein in the mitochondrion is further supported by previous proteomic work.[15] While GDP-mannose 4,6-dehydratase was not localized in TrypTag analysis and earlier studies have indicated its glycosomal location,[36] it was also identified in the mitoproteome previously.[15] Given the mitochondrial prediction from our screen and other work, further direct investigations might usefully determine whether the fucose synthesis pathway indeed exhibits dual localization and assist understanding the functional connection between cytoplasm and organelles.

Localization of 11 proteins to the mitochondrion matrix in addition to the cytoplasm or nucleus is intriguing. Although dual-localization conclusions based on protein tagging should be treated with caution (see above), four of our examples are validated from either existing literature or functional annotation, suggesting such moonlighting proteins are genuine.[68,69] Perhaps the best example is aconitase, dually present in the cytoplasm and mitochondrion in *T. brucei* and several unrelated species.[54] In yeast, aconitase has a specific targeting signal close to its C terminus that facilitates efficient post-translational targeting from the cytosol to the mitochondrion, which is sufficient and necessary for dual targeting. How dual localization is achieved in *T. brucei* is currently unknown.

In conclusion, we have used our in-depth characterization of tagging data to determine the comprehensive *T. brucei* mitoproteome, including mitochondrial sub-compartments as well as unique mitochondrial structures like the kinetoplast and the TAC, thus representing the largest high-confidence mitochondrial dissection to date. We additionally mapped an organelle-wide screening for which protein terminus is necessary for protein targeting. The data generated from this study enable diverse new discoveries about this well-studied organelle (Figure S5). Such findings have implications beyond kinetoplastid flagellates, providing a foundational resource for mitoproteins across eukaryotes and will inform future hypothesis-driven studies in diverse organisms.

Limitations of the study

Endogenous tagging carries concerns of altered gene expression levels when compared to untagged cell lines. While different expression can, in certain instances, induce altered localization patterns, we note the extreme correlation of organelle marker proteins throughout the TrypTag study, which in turn suggests that expression-induced mislocalizations are unlikely to be encountered in MitoTag. Furthermore, TrypTag analysis performed by Billington et al.[17] suggested that genes tagged in TrypTag display expression levels that correlated with the wild-type cell line despite UTR replacement. As noted above, comprehensive tagging is limited by applicability in that not all proteins are amenable to the attachment of foreign epitopes. While we have endeavored to employ this phenomenon productively, several canonical mitoproteins could not be verified in this manner due to failed cell line generation.

STAR★METHODS

Detailed methods are provided in the online version of this paper and include the following:

- KEY RESOURCES TABLE
- RESOURCE AVAILABILITY
  - Lead contact
  - Materials availability
  - Data and code availability
- EXPERIMENTAL MODEL AND STUDY PARTICIPANT DETAILS
- METHOD DETAILS
  - Mitochondrial protein identification
  - Cell culturing and *in situ* tagging
  - Kinetoplast proximity enrichment analysis (KPE)
  - Kinetoplast distance measurement
  - Split GFP and flow cytometry
- QUANTIFICATION AND STATISTICAL ANALYSIS

SUPPLEMENTAL INFORMATION

Supplemental information can be found online at https://doi.org/10.1016/j.celrep.2023.113083.

ACKNOWLEDGMENTS

This research was funded by the Czech Grant Agency projects 21-09283S and 21-19664S, the Gordon and Betty Moore Foundation GBMF#9354, ERD project OPVVV/0000759, Wellcome Trust Biomedical Resource Grant 108445/Z/15/Z, Wellcome Trust Investigator Award 214298/Z/18/Z, and Wellcome Trust Sir Henry Dale Fellowship 211075/Z/18/Z. For the purpose of open access, the author has applied a CC BY public copyright licence to any Author Accepted Manuscript version arising from this submission.

AUTHOR CONTRIBUTIONS

Conceptualization, J.P., S.D., J.D.S., R.J.W., and J.L.; software, R.J.W.; investigation, J.P., A.A., and R.J.W.; writing – original draft, J.P., M.H., S.D., J.D.S., R.J.W., K.G., and J.L.; visualization, J.P. and M.H.; funding acquisition, K.G. and J.L.; resources, K.G. and J.L.; supervision, S.D., J.P., R.J.W., and J.L.

DECLARATION OF INTERESTS

The authors declare no competing interests.

Received: March 19, 2023
Revised: June 30, 2023
Accepted: August 17, 2023

REFERENCES

1. Jensen, R.E., and Englund, P.T. (2012). Network news: The replication of kinetoplast DNA. Annu. Rev. Microbiol. *66*, 473–491. https://doi.org/10.1146/annurev-micro-092611-150057.
2. Ziemann, H. (1898). Eine methode der doppelfarbung bei Flagellaten, Pilzen, Spirillen und Bakterien, sowie bei einigen Amoben. Zentralbl Bakt Parasitenkd Infekt *24*, 945–955.
3. Benne, R., Van Den Burg, J., Brakenhoff, J.P., Sloof, P., Van Boom, J.H., and Tromp, M.C. (1986). Major transcript of the frameshifted coxII gene from trypanosome mitochondria contains four nucleotides that are not encoded in the DNA. Cell *46*, 819–826. https://doi.org/10.1016/0092-8674(86)90063-2.
4. Lukeš, J., Kaur, B., and Speijer, D. (2021). RNA editing in mitochondria and plastids: weird and widespread. Trends Genet. *37*, 99–102. https://doi.org/10.1016/j.tig.2020.10.004.
5. Pagliarini, D.J., Calvo, S.E., Chang, B., Sheth, S.A., Vafai, S.B., Ong, S.E., Walford, G.A., Sugiana, C., Boneh, A., Chen, W.K., et al. (2008). A mitochondrial protein compendium elucidates complex I disease biology. Cell *134*, 112–123. https://doi.org/10.1016/j.cell.2008.06.016.
6. Bílý, T., Sheikh, S., Mallet, A., Bastin, P., Pérez-Morga, D., Lukeš, J., and Hashimi, H. (2021). Ultrastructural changes of the mitochondrion during the life cycle of *Trypanosoma brucei*. J. Eukaryot. Microbiol. *68*, e12846. https://doi.org/10.1111/jeu.12846.
7. Zíková, A., Verner, Z., Nenarokova, A., Michels, P.A.M., and Lukeš, J. (2017). A paradigm shift: The mitoproteomes of procyclic and bloodstream *Trypanosoma brucei* are comparably complex. PLoS Pathog. *13*, e1006679. https://doi.org/10.1371/journal.ppat.1006679.
8. Schneider, A. (2018). Mitochondrial protein import in trypanosomatids: Variations on a theme or fundamentally different? PLoS Pathog. *14*, e1007351. https://doi.org/10.1371/journal.ppat.1007351.
9. Ramrath, D.J.F., Niemann, M., Leibundgut, M., Bieri, P., Prange, C., Horn, E.K., Leitner, A., Boehringer, D., Schneider, A., and Ban, N. (2018). Evolutionary shift toward protein-based architecture in trypanosomal mitochondrial ribosomes. Science *362*, eaau7735. https://doi.org/10.1126/science.aau7735.
10. Acestor, N., Zíková, A., Dalley, R.A., Anupama, A., Panigrahi, A.K., and Stuart, K.D. (2011). *Trypanosoma brucei* mitochondrial respiratome: Composition and organization in procyclic form. Mol. Cell. Proteomics *10*, M110.006908. https://doi.org/10.1074/mcp.M110.006908.
11. Lai, D.H., Hashimi, H., Lun, Z.R., Ayala, F.J., and Lukeš, J. (2008). Adaptations of *Trypanosoma brucei* to gradual loss of kinetoplast DNA: *Trypanosoma equiperdum* and *Trypanosoma evansi* are petite mutants of *T. brucei*. Proc. Natl. Acad. Sci. USA. *105*, 1999–2004. https://doi.org/10.1073/pnas.0711799105.
12. Amodeo, S., Bregy, I., and Ochsenreiter, T. (2022). Mitochondrial genome maintenance - the kinetoplast story. FEMS Microbiol. Rev.fuac047 https://doi.org/10.1093/femsre/fuac047.
13. Panigrahi, A.K., Ogata, Y., Zíková, A., Anupama, A., Dalley, R.A., Acestor, N., Myler, P.J., and Stuart, K.D. (2009). A comprehensive analysis of *Trypanosoma brucei* mitochondrial proteome. Proteomics *9*, 434–450. https://doi.org/10.1002/pmic.200800477.
14. Acestor, N., Panigrahi, A.K., Ogata, Y., Anupama, A., and Stuart, K.D. (2009). Protein composition of *Trypanosoma brucei* mitochondrial membranes. Proteomics *9*, 5497–5508. https://doi.org/10.1002/pmic.200900354.
15. Peikert, C.D., Mani, J., Morgenstern, M., Käser, S., Knapp, B., Wenger, C., Harsman, A., Oeljeklaus, S., Schneider, A., and Warscheid, B. (2017). Charting organellar importomes by quantitative mass spectrometry. Nat. Commun. *8*, 15272. https://doi.org/10.1038/ncomms15272.
16. Shaner, N.C., Lambert, G.G., Chammas, A., Ni, Y., Cranfill, P.J., Baird, M.A., Sell, B.R., Allen, J.R., Day, R.N., Israelsson, M., et al. (2013). A bright monomeric green fluorescent protein derived from *Branchiostoma lanceolatum*. Nat. Methods *10*, 407–409. https://doi.org/10.1038/nmeth.2413.
17. Billington, K., Halliday, C., Madden, R., Dyer, P., Barker, A.R., Moreira-Leite, F.F., Carrington, M., Vaughan, S., Hertz-Fowler, C., Dean, S., et al. (2023). Genome-wide subcellular protein map for the flagellate parasite *Trypanosoma brucei*. Nat. Microbiol. *8*, 533–547. https://doi.org/10.1038/s41564-022-01295-6.
18. Meurer, M., Duan, Y., Sass, E., Kats, I., Herbst, K., Buchmuller, B.C., Dederer, V., Huber, F., Kirrmaier, D., Štefl, M., et al. (2018). Genome-wide C-SWAT library for high-throughput yeast genome tagging. Nat. Methods *15*, 598–600. https://doi.org/10.1038/s41592-018-0045-8.
19. Huh, W.K., Falvo, J.V., Gerke, L.C., Carroll, A.S., Howson, R.W., Weissman, J.S., and O'Shea, E.K. (2003). Global analysis of protein localization in budding yeast. Nature *425*, 686–691. https://doi.org/10.1038/NATURE02026.
20. Hayashi, A., Ding, D.Q., Tsutsumi, C., Chikashige, Y., Masuda, H., Haraguchi, T., and Hiraoka, Y. (2009). Localization of gene products using a chromosomally tagged GFP-fusion library in the fission yeast *Schizosaccharomyces pombe*. Genes Cell. *14*, 217–225. https://doi.org/10.1111/J.1365-2443.2008.01264.X.
21. Klingbeil, M.M., Motyka, S.A., and Englund, P.T. (2002). Multiple mitochondrial DNA polymerases in *Trypanosoma brucei*. Mol. Cell *10*, 175–186. https://doi.org/10.1016/S1097-2765(02)00571-3.
22. Saxowsky, T.T., Choudhary, G., Klingbeil, M.M., and Englund, P.T. (2003). *Trypanosoma brucei* has two distinct mitochondrial DNA polymerase beta enzymes. J. Biol. Chem. *278*, 49095–49101. https://doi.org/10.1074/jbc.M308565200.
23. Liu, B., Molina, H., Kalume, D., Pandey, A., Griffith, J.D., and Englund, P.T. (2006). Role of p38 in replication of *Trypanosoma brucei* kinetoplast DNA. Mol. Cell Biol. *26*, 5382–5393. https://doi.org/10.1128/mcb.00369-06.
24. Downey, N., Hines, J.C., Sinha, K.M., and Ray, D.S. (2005). Mitochondrial DNA ligases of *Trypanosoma brucei*. Eukaryot. Cell *4*, 765–774. https://doi.org/10.1128/ec.4.4.765-774.2005.
25. Pyrih, J., Rašková, V., Škodová-Sveráková, I., Pánek, T., and Lukeš, J. (2020). ZapE/Afg1 interacts with Oxa1 and its depletion causes a multifaceted phenotype. PLoS One *15*, e0234918. https://doi.org/10.1371/journal.pone.0234918.
26. Zíková, A., Panigrahi, A.K., Dalley, R.A., Acestor, N., Anupama, A., Ogata, Y., Myler, P.J., and Stuart, K. (2008). *Trypanosoma brucei* mitochondrial ribosomes. Mol. Cell. Proteomics *7*, 1286–1296. https://doi.org/10.1074/mcp.m700490-mcp200.
27. Niemann, M., Wiese, S., Mani, J., Chanfon, A., Jackson, C., Meisinger, C., Warscheid, B., and Schneider, A. (2013). Mitochondrial outer membrane proteome of *Trypanosoma brucei* reveals novel factors required to maintain mitochondrial morphology. Mol. Cell. Proteomics *12*, 515–528. https://doi.org/10.1074/mcp.M112.023093.
28. Zíková, A., Schnaufer, A., Dalley, R.A., Panigrahi, A.K., and Stuart, K.D. (2009). The F0F1-ATP synthase complex contains novel subunits and is essential for procyclic *Trypanosoma brucei*. PLoS Pathog. *5*, e1000436. https://doi.org/10.1371/JOURNAL.PPAT.1000436.
29. Aphasizheva, I., Alfonzo, J., Carnes, J., Cestari, I., Cruz-Reyes, J., Göringer, H.U., Hajduk, S., Lukeš, J., Madison-Antenucci, S., Maslov, D.A., et al. (2020). Lexis and grammar of mitochondrial RNA processing in trypanosomes. Trends Parasitol. *36*, 337–355. https://doi.org/10.1016/j.pt.2020.01.006.

30. Harsman, A., and Schneider, A. (2017). Mitochondrial protein import in trypanosomes: Expect the unexpected. Traffic *18*, 96–109. https://doi.org/10.1111/tra.12463.

31. Ducker, G.S., and Rabinowitz, J.D. (2017). One-carbon metabolism in health and disease. Cell Metab. *25*, 27–42. https://doi.org/10.1016/j.cmet.2016.08.009.

32. Lawrence, S.A., Titus, S.A., Ferguson, J., Heineman, A.L., Taylor, S.M., and Moran, R.G. (2014). Mammalian mitochondrial and cytosolic folylpolyglutamate synthetase maintain the subcellular compartmentalization of folates. J. Biol. Chem. *289*, 29386–29396. https://doi.org/10.1074/jbc.M114.593244.

33. Anderson, D.D., Quintero, C.M., and Stover, P.J. (2011). Identification of a de novo thymidylate biosynthesis pathway in mammalian mitochondria. Proc. Natl. Acad. Sci. USA. *108*, 15163–15168. https://doi.org/10.1073/pnas.1103623108.

34. Vickers, T.J., and Beverley, S.M. (2011). Folate metabolic pathways in *Leishmania*. Essays Biochem. *51*, 63–80. https://doi.org/10.1042/BSE0510063.

35. Moro-Bulnes, A., Castillo-Acosta, V.M., Valente, M., Carrero-Lérida, J., Pérez-Moreno, G., Ruiz-Pérez, L.M., and González-Pacanowska, D. (2019). Contribution of cytidine deaminase to thymidylate biosynthesis in *Trypanosoma brucei*: Intracellular localization and properties of the enzyme. mSphere *4*, e003744-19. https://doi.org/10.1128/msphere.00374-19.

36. Turnock, D.C., Izquierdo, L., and Ferguson, M.A.J. (2007). The de novo synthesis of GDP-fucose is essential for flagellar adhesion and cell growth in *Trypanosoma brucei*. J. Biol. Chem. *282*, 28853–28863. https://doi.org/10.1074/jbc.M704742200.

37. Sampaio Guther, M.L., Prescott, A.R., Kuettel, S., Tinti, M., and Ferguson, M.A.J. (2021). Nucleotide sugar biosynthesis occurs in the glycosomes of procyclic and bloodstream form *Trypanosoma brucei*. PLoS Negl. Trop. Dis. *15*, e0009132. https://doi.org/10.1371/journal.pntd.0009132.

38. Becker, D.J., and Lowe, J.B. (2003). Fucose: Biosynthesis and biological function in mammals. Glycobiology *13*, 41R–53R. https://doi.org/10.1093/glycob/cwg054.

39. Bandini, G., Damerow, S., Sempaio Guther, M.L., Guo, H., Mehlert, A., Paredes Franco, J.C., Beverley, S., and Ferguson, M.A. (2021). An essential, kinetoplastid-specific GDP-FUC: P-d-gal a-1,2- fucosyltransferase is located in the mitochondrion of *Trypanosoma brucei*. eLife *10*, e70272. https://doi.org/10.7554/eLife.70272.

40. Guo, H., Damerow, S., Penha, L., Menzies, S., Polanco, G., Zegzouti, H., Ferguson, M.A.J., and Beverley, S.M. (2021). A broadly active fucosyltransferase LmjFUT1 whose mitochondrial localization and activity are essential in parasitic *Leishmania*. Proc. Natl. Acad. Sci. USA. *118*, e2108963118. https://doi.org/10.1073/pnas.2108963118.

41. Schneider, A., and Ochsenreiter, T. (2018). Failure is not an option - mitochondrial genome segregation in trypanosomes. J. Cell Sci. *131*, jcs221820. https://doi.org/10.1242/jcs.221820.

42. Yagüe-Capilla, M., Castillo-Acosta, V.M., Bosch-Navarrete, C., Ruiz-Pérez, L.M., and González-Pacanowska, D. (2021). A mitochondrial orthologue of the dNTP triphosphohydrolase SAMHD1 is essential and controls pyrimidine homeostasis in *Trypanosoma brucei*. ACS Infect. Dis. *7*, 318–332. https://doi.org/10.1021/acsinfecdis.0c00551.

43. Hoffmann, A., Käser, S., Jakob, M., Amodeo, S., Peitsch, C., Týč, J., Vaughan, S., Zuber, B., Schneider, A., and Ochsenreiter, T. (2018). Molecular model of the mitochondrial genome segregation machinery in *Trypanosoma brucei*. Proc. Natl. Acad. Sci. USA. *115*, E1809–E1818. https://doi.org/10.1073/pnas.1716582115.

44. Baudouin, H.C.M., Pfeiffer, L., and Ochsenreiter, T. (2020). A comparison of three approaches for the discovery of novel tripartite attachment complex proteins in *Trypanosoma brucei*. PLoS Negl. Trop. Dis. *14*, e0008568. https://doi.org/10.1371/journal.pntd.0008568.

45. Wiedemann, N., and Pfanner, N. (2017). Mitochondrial machineries for protein import and assembly. Annu. Rev. Biochem. *86*, 685–714. https://doi.org/10.1146/annurev-biochem-060815-014352.

46. Schneider, A. (2022). Evolution and diversification of mitochondrial protein import systems. Curr. Opin. Cell Biol. *75*, 102077. https://doi.org/10.1016/J.CEB.2022.102077.

47. Brix, J., Dietmeier, K., and Pfanner, N. (1997). Differential recognition of preproteins by the purified cytosolic domains of the mitochondrial import receptors Tom20, Tom22, and Tom70. J. Biol. Chem. *272*, 20730–20735. https://doi.org/10.1074/jbc.272.33.20730.

48. Rampelt, H., Sucec, I., Bersch, B., Horten, P., Perschil, I., Martinou, J.C., Van Der Laan, M., Wiedemann, N., Schanda, P., and Pfanner, N. (2020). The mitochondrial carrier pathway transports non-canonical substrates with an odd number of transmembrane segments. BMC Biol. *18*, 2. https://doi.org/10.1186/s12915-019-0733-6.

49. Ohara-Imaizumi, M., Yoshida, M., Aoyagi, K., Saito, T., Okamura, T., Takenaka, H., Akimoto, Y., Nakamichi, Y., Takanashi-Yanobu, R., Nishiwaki, C., et al. (2010). Deletion of CDKAL1 affects mitochondrial ATP generation and first-phase insulin exocytosis. PLoS One *5*, e15553. https://doi.org/10.1371/journal.pone.0015553.

50. Wei, F.Y., Suzuki, T., Watanabe, S., Kimura, S., Kaitsuka, T., Fujimura, A., Matsui, H., Atta, M., Michiue, H., Fontecave, M., et al. (2011). Deficit of tRNALys modification by Cdkal1 causes the development of type 2 diabetes in mice. J. Clin. Invest. *121*, 3598–3608. https://doi.org/10.1172/JCI58056.

51. Brambillasca, S., Altkrueger, A., Colombo, S.F., Friederich, A., Eickelmann, P., Mark, M., Borgese, N., and Solimena, M. (2012). CDK5 regulatory subunit-associated protein 1-like 1 (CDKAL1) is a tail-anchored protein in the endoplasmic reticulum (ER) of insulinoma cells. J. Biol. Chem. *287*, 41808–41819. https://doi.org/10.1074/jbc.M112.376558.

52. Bogacz, M., and Krauth-Siegel, R.L. (2018). Tryparedoxin peroxidase-deficiency commits trypanosomes to ferroptosis-type cell death. eLife *7*, e37503. https://doi.org/10.7554/ELIFE.37503.

53. Ebersoll, S., Bogacz, M., Günter, L.M., Dick, T.P., and Krauth-Siegel, R.L. (2020). A tryparedoxin-coupled biosensor reveals a mitochondrial trypanothione metabolism in trypanosomes. eLife *9*, e53227. 10.7554/eLife.53227.

54. Saas, J., Ziegelbauer, K., Von Haeseler, A., Fast, B., and Boshart, M. (2000). A developmentally regulated aconitase related to iron-regulatory protein-1 is localized in the cytoplasm and in the mitochondrion of *Trypanosoma brucei*. J. Biol. Chem. *275*, 2745–2755. https://doi.org/10.1074/jbc.275.4.2745.

55. Van Hellemond, J.J., Opperdoes, F.R., and Tielens, A.G.M. (2005). The extraordinary mitochondrion and unusual citric acid cycle in *Trypanosoma brucei*. Biochem. Soc. Trans. *33*, 967–971. https://doi.org/10.1042/BST20050967.

56. Van Weelden, S.W.H., Fast, B., Vogt, A., Van der Meer, P., Saas, J., Van Hellemond, J.J., Tielens, A.G.M., and Boshart, M. (2003). Procyclic *Trypanosoma brucei* do not use Krebs cycle activity for energy generation. J. Biol. Chem. *278*, 12854–12863. https://doi.org/10.1074/jbc.M213190200.

57. Wang, X., Inaoka, D.K., Shiba, T., Balogun, E.O., Allmann, S., Watanabe, Y.I., Boshart, M., Kita, K., and Harada, S. (2017). Expression, purification, and crystallization of type 1 isocitrate dehydrogenase from *Trypanosoma brucei brucei*. Protein Expr. Purif. *138*, 56–62. https://doi.org/10.1016/j.pep.2017.06.011.

58. Hammond, M.J., Nenarokova, A., Butenko, A., Zoltner, M., Lacová Dobáková, E., Field, M.C., and Lukeš, J. (2020). A uniquely complex mitochondrial proteome from *Euglena gracilis*. Mol. Biol. Evol. *37*, 2173–2191. https://doi.org/10.1093/MOLBEV/MSAA061.

59. Smith, A.C., and Robinson, A.J. (2019). MitoMiner v4.0: an updated database of mitochondrial localization evidence, phenotypes and diseases. Nucleic Acids Res. *47*, D1225–D1228. https://doi.org/10.1093/NAR/GKY1072.

60. Liu, B., Wang, J., Yaffe, N., Lindsay, M.E., Zhao, Z., Zick, A., Shlomai, J., and Englund, P.T. (2009). Trypanosomes have six mitochondrial DNA helicases with one controlling kinetoplast maxicircle replication. Mol. Cell *35*, 490–501. https://doi.org/10.1016/j.molcel.2009.07.004.

61. Ochsenreiter, T., Anderson, S., Wood, Z.A., and Hajduk, S.L. (2008). Alternative RNA editing produces a novel protein involved in mitochondrial DNA maintenance in trypanosomes. Mol. Cell Biol. *28*, 5595–5604. https://doi.org/10.1128/mcb.00637-08.

62. Engel, M.L., and Ray, D.S. (1999). The kinetoplast structure-specific endonuclease I is related to the 5' exo/endonuclease domain of bacterial DNA polymerase I and colocalizes with the kinetoplast topoisomerase II and DNA polymerase beta during replication. Proc. Natl. Acad. Sci. USA. *96*, 8455–8460. https://doi.org/10.1073/PNAS.96.15.8455.

63. Wong, R.G., Kazane, K., Maslov, D.A., Rogers, K., Aphasizhev, R., and Simpson, L. (2015). U-insertion/deletion RNA editing multiprotein complexes and mitochondrial ribosomes in *Leishmania tarentolae* are located in antipodal nodes adjacent to the kinetoplast DNA. Mitochondrion *25*, 76–86. https://doi.org/10.1016/J.MITO.2015.10.006.

64. Panov, A., and Orynbayeva, Z. (2013). Bioenergetic and antiapoptotic properties of mitochondria from cultured human prostate cancer cell lines PC-3, DU145 and LNCaP. PLoS One *8*, e72078. https://doi.org/10.1371/JOURNAL.PONE.0072078.

65. Basler, G., Grimbs, S., and Nikoloski, Z. (2012). Optimizing metabolic pathways by screening for feasible synthetic reactions. Biosystems *109*, 186–191. https://doi.org/10.1016/J.BIOSYSTEMS.2012.04.007.

66. Marchese, L., Nascimento, J.D.F., Damasceno, F.S., Bringaud, F., Michels, P.A.M., and Silber, A.M. (2018). The uptake and metabolism of amino acids, and their unique role in the biology of pathogenic trypanosomatids. Pathogens *7*, 36. https://doi.org/10.3390/pathogens7020036.

67. Johnston, K., Kim, D.H., Kerkhoven, E., Burchmore, R., Barrett, M., and Achcar, F. (2019). Mapping the metabolism of five amino acids in bloodstream form *Trypanosoma brucei* using U-13C-labelled substrates and LC–MS. Biosci. Rep. *39*, 20181601. https://doi.org/10.1042/BSR20181601/219173.

68. Paris, Z., Horáková, E., Rubio, M.A.T., Sample, P., Fleming, I.M.C., Armocida, S., Lukeš, J., and Alfonzo, J.D. (2013). The *T. brucei* TRM5 methyltransferase plays an essential role in mitochondrial protein synthesis and function. RNA *19*, 649–658. https://doi.org/10.1261/rna.036665.112.

69. Furtado, C., Kunrath-Lima, M., Rajão, M.A., Mendes, I.C., de Moura, M.B., Campos, P.C., Macedo, A.M., Franco, G.R., Pena, S.D.J., Teixeira, S.M.R., et al. (2012). Functional characterization of 8-oxoguanine DNA glycosylase of *Trypanosoma cruzi*. PLoS One *7*, 42484. https://doi.org/10.1371/journal.pone.0042484.

70. Panigrahi, A.K., Zíková, A., Dalley, R.A., Acestor, N., Ogata, Y., Anupama, A., Myler, P.J., and Stuart, K.D. (2008). Mitochondrial complexes in *Trypanosoma brucei*: A novel complex and a unique oxidoreductase complex. Mol. Cell. Proteomics *7*, 534–545. https://doi.org/10.1074/mcp.M700430-MCP200.

71. Poon, S.K., Peacock, L., Gibson, W., Gull, K., and Kelly, S. (2012). A modular and optimized single marker system for generating *Trypanosoma brucei* cell lines expressing T7 RNA polymerase and the tetracycline repressor. Open Biol. *2*, 110037. https://doi.org/10.1098/rsob.110037.

72. Kaurov, I., Vancová, M., Schimanski, B., Cadena, L.R., Heller, J., Bílý, T., Potěšil, D., Eichenberger, C., Bruce, H., Oeljeklaus, S., et al. (2018). The diverged trypanosome MICOS complex as a hub for mitochondrial cristae shaping and protein import. Curr. Biol. *28*, 3393–3407.e5. https://doi.org/10.1016/j.cub.2018.09.008.

73. Paterou, A., Týč, J., Sunter, J., Vaughan, S., Gull, K., and Dean, S. (2023). Unlocking trypanosome biology: a comprehensive protein-tagging toolkit for localization and functional analysis. bioRxiv, 04.21.537815. https://doi.org/10.1101/2023.04.21.537815.

74. Alves, A.A., Gabriel, H.B., Bezerra, M.J.R., de Souza, W., Vaughan, S., Cunha-E-Silva, N.L., and Sunter, J.D. (2020). Control of assembly of extra-axonemal structures: The paraflagellar rod of trypanosomes. J. Cell Sci. *133*, jcs242271. https://doi.org/10.1242/jcs.242271.

75. Käll, L., Krogh, A., and Sonnhammer, E.L.L. (2004). A combined transmembrane topology and signal peptide prediction method. J. Mol. Biol. *338*, 1027–1036. https://doi.org/10.1016/J.JMB.2004.03.016.

76. Krogh, A., Larsson, B., Von Heijne, G., and Sonnhammer, E.L. (2001). Predicting transmembrane protein topology with a hidden Markov model: Application to complete genomes. J. Mol. Biol. *305*, 567–580. https://doi.org/10.1006/jmbi.2000.4315.

77. Halliday, C., Billington, K., Wang, Z., Madden, R., Dean, S., Sunter, J.D., and Wheeler, R.J. (2019). Cellular landmarks of *Trypanosoma brucei* and *Leishmania mexicana*. Mol. Biochem. Parasitol. *230*, 24–36. https://doi.org/10.1016/j.molbiopara.2018.12.003.

78. Dean, S., Sunter, J.D., and Wheeler, R.J. (2017). TrypTag.org: A trypanosome genome-wide protein localisation resource. Trends Parasitol. *33*, 80–82. https://doi.org/10.1016/j.pt.2016.10.009.

79. Wheeler, R.J. (2020). ImageJ for partially and fully automated analysis of trypanosome micrographs. Methods Mol. Biol. *2116*, 385–408. https://doi.org/10.1007/978-1-0716-0294-2_24/COVER/.

80. López-Escobar, L., Hänisch, B., Halliday, C., Ishii, M., Akiyoshi, B., Dean, S., Daniel Sunter, J., John Wheeler, R., and Gull, K. (2022). Stage-specific transcription activator ESB1 regulates monoallelic antigen expression in *Trypanosoma brucei*. Nat. Microbiol. *7*, 1280–1290. https://doi.org/10.1038/s41564-022-01175-z.

81. Kelly, S., Reed, J., Kramer, S., Ellis, L., Webb, H., Sunter, J., Salje, J., Marinsek, N., Gull, K., Wickstead, B., and Carrington, M. (2007). Functional genomics in *Trypanosoma brucei*: a collection of vectors for the expression of tagged proteins from endogenous and ectopic gene loci. Mol. Biochem. Parasitol. *154*, 103–109. https://doi.org/10.1016/J.MOLBIOPARA.2007.03.012.

STAR★METHODS

KEY RESOURCES TABLE

REAGENT or RESOURCE	SOURCE	IDENTIFIER
Antibodies		
Rabbit anti-V5	Sigma Aldrich	Catalog #: V8137; RRID: AB_261889 (https://antibodyregistry.org/search.php?q=AB_261889)
Mouse anti-HSP70	Panigrahi et al.[70]	
Goat anti-Rabbit IgG (H + L) Highly Cross-Adsorbed Secondary Antibody, Alexa Fluor™ Plus 488	ThermoScientific (LifeTechnologies)	Catalog # A32731; RRID: AB_2633280 (https://www.thermofisher.com/antibody/product/Goat-anti-Rabbit-IgG-H-L-Highly-Cross-Adsorbed-Secondary-Antibody-Polyclonal/A32731)
Goat anti-Mouse IgG (H + L) Highly Cross-Adsorbed Secondary Antibody, Alexa Fluor™ Plus 555	ThermoScientific (LifeTechnologies)	Catalog # A32727; RRID: AB_2633276 (https://www.thermofisher.com/antibody/product/Goat-anti-Mouse-IgG-H-L-Highly-Cross-Adsorbed-Secondary-Antibody-Polyclonal/A32727)
Chemicals, peptides, and recombinant proteins		
MitoTracker™ Red CMXRos	ThermoScientific (LifeTechnologies)	Catalog #: M7512
MitoTracker™ Green FM	ThermoScientific (LifeTechnologies)	Catalog #: M7514
HaloTag® TMR Ligand	Promega	Catalog #: G8252
Q5 High-Fidelity DNA Polymerase	New England Biolabs	Catalog #: M0491
Critical commercial assays		
Direct-zol RNA MiniPrep w/Zymo-Spin IIC Columns	Zymo Research (Amplicon)	Catalog #: R2050
Human T cell Nucleofector Kit, 100 reactions	Lonza	Catalog #: VVPA-1002
Bolt TM 4–12% Bis-Tris Plus Gels	ThermoScientific (LifeTechnologies)	Catalog #: NW04120BOX
Deposited data		
Source images for Figures 3, 4, 5, 6, and 7	TrypTag database, Billington et al.[17]	http://tryptag.org/
Raw data from Figure 2, S2, and S3	Mendeley data	https://doi.org/10.17632/4f7mbvdc6b.1
Source images for MitoTag proteome analysis	TrypTag database, Billington et al.[17]	http://tryptag.org/
Experimental models: Cell lines		
For cell lines used in this study, see Table S1I		
Experimental models: Organisms/strains		
SMOXP9 T. brucei cell line	Poon et al.[71]	RRID: SCR_004786
Oligonucleotides		
For oligonucleotides used in this study, see Table S1I		N/A
Recombinant DNA		
pPOT-V5-HygR	Kaurov et al.[72]	N/A
pPOT7 mNG	Paterou et al.[73]	https://www.biorxiv.org/content/10.1101/2023.04.21.537815v1
pPOT6 mNG, eGFP, eYFP, TagRFPt, HaloTag, tdTomato	Paterou et al.[73]	https://www.biorxiv.org/content/10.1101/2023.04.21.537815v1
pPOT6 mNGV5	This study	N/A
pPOTv7-G418-spGFP11	This study	N/A

(*Continued on next page*)

Continued

REAGENT or RESOURCE	SOURCE	IDENTIFIER
pJ1313	Alves et al.[74]	N/A
pJ1358	This study	N/A
Software and algorithms		
Microsoft Excel	Microsoft	https://www.microsoft.com
ImageJ 1.5x, Micro-Manager plugin 1.4.23	ImageJ	https://imagej.nih.gov/ij/index.html
FlowJo_v10.8.0	FlowJo	https://www.flowjo.com/
Phobius	Käll et al.[75]	http://phobius.sbc.su.se/
TMHMM	Krogh et al.[76]	https://services.healthtech.dtu.dk/service.php?TMHMM-2.0

RESOURCE AVAILABILITY

Lead contact

Further information and requests for resources and reagents should be directed to and will be fulfilled by the lead contact, Jan Pyrih (jan.pyrih@gmail.com).

Materials availability

Plasmid pPOT6 mNGV5 and novel cell lines generated in this study are available from the lead contact upon request. All unique/stable reagents generated in this study are available from the lead contact with a completed materials transfer agreement.

Data and code availability

- This paper analyzes existing, publicly available data. These datasets are listed in the Key resources table. All additional data needed to evaluate the conclusions in the paper are present in the paper and/or the Supplementary Materials. Raw image data from Figure 2, S2, and S3 have been deposited at Mendeley data and are publicly available as of the date of publication. DOIs are listed in the Key resources table.
- This paper does not report original code.
- Any additional information required to reanalyze the data reported in this work paper is available from the lead contact upon request.

EXPERIMENTAL MODEL AND STUDY PARTICIPANT DETAILS

The procyclic T. brucei (RRID: SCR_004786) 927 strain SmOxP cell line served as the parental cell line for all experiments. It was grown at 27°C in SDM79 medium supplemented with 10% fetal bovine serum.

METHOD DETAILS

Mitochondrial protein identification

The TrypTag mitoproteome (MitoTag) was defined as the set of proteins where TrypTag showed a mitochondrial localization by N- and/or C-terminal tagging[17,77] (Figure S1). For comparison to existing mitoproteomes, other proteins were classified as either: ''Non-mitochondrial'' or ''No evidence/Unknown''. ''Non-mitochondrial'' refers to a convincing fluorescent signal in the cytoplasm or at a non-mitochondrial organelle or structure, based on the majority of cells in the population. ''No evidence/Unknown'' was applied to proteins where tagging was not attempted, generation of tagging data was unsuccessful or where the tagged cell line had only background fluorescence signal intensity (i.e., a faint punctate or reticulated signal similar to parental cell line) as determined by automated signal measurement employed by TrypTag.[17]

Cell culturing and *in situ* tagging

For generation of additional tagged cell lines, procyclic stage *T. brucei* SmOx 927[71] was grown at 27°C in SDM79 medium supplemented with 10% fetal bovine serum. Genes of interest were tagged as described previously[78] using pPOTv5, pPOTv6 or pPOTv7 plasmids (see Table S1I).[72,73] One additional version of pPOTv6 tagging plasmid (pPOTv6_mNG::V5_BLAST) was created by the insertion of sequence corresponding to three V5 tag repetitions into BamHI/SacI restricted pPOTv6_mNG_BLAST plasmid[73] using primers described in Table S1I. An IscU target peptide was identified according to a former study,[25] and one genomic copy of the IscU gene was targeted for truncation using mNeonGreen pPOTv7 plasmid as PCR-tagging template.

Kinetoplast proximity enrichment analysis (KPE)

Images of cell lines were inspected for the presence of enrichment of fluorescence signal close to the kinetoplast (for characterization of KPE, see Results). At least two fields per cell line were inspected, and if KPE signal was detected in more than 5% of cells then it was classified as KPE. This allows for sensitive detection of KPE even in cell lines with low fluorescent signal intensity and allowing for imperfectly focused kinetoplasts. Cell lines with weak mitochondrial signal (mitochondrial annotation labeled "faint" by Billington et al.[17]) prevented confident detection of KPE and were therefore excluded from analysis (Figure S1).

We independently confirmed the identification of KPE signal using automated analysis. For each cell in cell lines with mitochondrial signal in the TrypTag dataset (typically ~250 cells per cell line), we measured the ratio of the brightest pixel within 7 pixels (0.7 μM) of the kinetoplast and the brightest pixel elsewhere in the cell in the mNG fluorescence image. For each cell line, if the 90th percentile of this list of ratios was >1.05, it was classified as possessing the KPE, i.e., if in at least 10% of the cells the brightest signal in the cell was within 0.7 μm of the kinetoplast. This was 94.1% specific and 90.9% sensitive on the test set of proteins in Figure 3B. Overall agreement with manual KPE classifications was 95.2% for the entire dataset, therefore all analyses used the manual classifications.

When KPE was identified, the protein was categorized as localizing to either the matrix or within the IMM. When no KPE was evident ("noKPE"; Figure S1), the protein was categorized as localizing either in the IMS, as an integral part of the OMM or proteins associated with the OMM, or in the outer side of the IMM. The proteins were subsequently classified as an IMM or OMM integral component when a transmembrane (TM) domain was predicted by either Phobius[75] or TMHMM.[76]

Kinetoplast distance measurement

Distances between the kinetoplast and kinetoplast-associated structures were measured for every cell in the relevant TrypTag images when the kinetoplast was identified as in-focus. The center point of the kinetoplast (blue fluorescence channel, Hoechst 33342 DNA stain) and point-like kinetoplast-associated structures (green fluorescence channel, mNG-tagged protein) were identified by fitting a Gaussian in X and Y in the blue and green channels.[79] Distance from the structure in which the tagged protein was present and the kinetoplast was taken as the Euclidean distance between these center points. This setup gives us a resolution of <50 nm, similar to previous analyses.[80]

Split GFP and flow cytometry

A constitutive expression plasmid (pJ1313) was generated from p3605 by replacing the eYFP open reading frame (ORF) with a 3Ty-mNG-3Ty ORF and with the removal of additional *Spe*I sites to enable simple generation of N- and C-terminally tagged proteins using the same strategy as for the pDEX577 plasmid.[81] The GFP1-10 construct was amplified with the forward primer, including the IscU target peptide and cloned into pJ1313[74] using the *Hind*III/*BamH*I restriction sites to generate pJ1358. *Pac*I was used to linearise this plasmid, which was subsequently transfected into SmOxP9 cells and selected with blasticidin at a concentration of 5 μg/mL.

GFP11 was cloned between the *Hind*III/*BamH*I sites of pPOTv7- G418-mNG using GFP11-encoding primers, generating a pPOTv7-G418-spGFP11. The resulting plasmid was used as a template for long primer PCR. Live cells were analyzed using the BD Accuri C6 flow cytometer with the 533/30 nm filter, with 50,000 events collected for each sample and the results analyzed with FlowJo. The whole cell population was measured. No gating for different cell types was applied. The measurement data are presented in Table S1E.

QUANTIFICATION AND STATISTICAL ANALYSIS

Microsoft Excel was used to calculate mean values and standard deviation. Information about its presence is included in the figure legends. In the graphs either individual values are displayed or the number of individual cells measured is indicated. Detailed information about how KPE enrichment was defined in our automated analysis is included in the method detail section above.